A Second-Order Bulk Boundary-Layer Model

DAVID A. RANDALL AND QINGQIU SHAO

Department of Atmospheric Science, Colorado State University, Fort Collins, Colorado

CHIN-HOH MOENG

National Center for Atmospheric Research, Boulder, Colorado*

(Manuscript received 26 December 1990, in final form 8 January 1992)

ABSTRACT

Bulk mass-flux models represent the large eddies that are primarily responsible for the turbulent fluxes in the planetary boundary layer as convective circulations, with an associated convective mass flux. In order for such models to be useful, it is necessary to determine the fractional area covered by rising motion in the convective circulations. This fraction can be used as an estimate of the cloud amount, under certain conditions. "Matching" conditions have been developed that relate the convective mass flux to the ventilation and entrainment mass fluxes. These are based on conservation equations for the scalar means and variances in the entrainment and ventilation layers. Methods are presented to determine both the fractional area covered by rising motion and the convective mass flux. The requirement of variance balance is used to relax the "well-mixed" assumption. The vertical structures of the mean state and the turbulent fluxes are determined analytically. Several aspects of this simple model's formulation are evaluated using results from large-eddy simulations.

1. Introduction

The "bulk" approach to parametric representation of boundary-layer processes in large-scale models, pioneered by Deardorff (1972) and further developed by Randall (1976), Benoit (1976), and Suarez et al. (1983), involves a simple planetary boundary layer (PBL) model in which some aspects of the vertical structure of the mean state are parameterized. Among the parameters introduced to represent the mean state are the PBL depth, which is prognostically determined, and "jumps" or discontinuities at the PBL top. The use of jumps amounts to a concession that, although the fine structure near the PBL top is important for the PBL physics, it is unresolvable by any grid that can be used in a large-scale model. Extensive results from a PBL parameterization based on a bulk model have been reported by Randall et al. (1985).

The key shortcomings of existing bulk models are their assumption of vertical homogeneity for conservative variables and their inability to predict fractional cloud amounts. In attempts to address these deficiencies, a number of recent studies (cited below) have made use of a convective mass-flux parameterization.

The mass-flux concept was invented for use in a cumulus parameterization by Arakawa (1969). It was later adapted to the problem of boundary-layer parameterization by Betts (1973, 1983), Albrecht et al. (1979), Hanson (1981), Penc and Albrecht (1986), Wang and Albrecht (1986, 1990), Randall (1987), and Chatfield and Brost (1987). We refer to bulk boundary-layer models that use the mass-flux concept as "bulk mass-flux models." In such models the convective mass flux is assumed to be associated with convective circulations that have ascending and descending branches. Several of the modeling studies just cited allow the possibility that cloudiness can occur (or not) in either branch. The concept of "convective circulations" has also been used in observational studies (based on conditional sampling or joint distribution functions, or both) by Lenschow and Stephens (1980, 1982), Greenhut and Khalsa (1982), Wilczak and Businger (1983), Mahrt and Paumier (1984), Grossman (1984), Khalsa and Greenhut (1985), Penc and Albrecht (1986), and Young (1988a,b). Recently, it has been applied to analyze the results of large-eddy simulations by Schmidt and Schumann (1989), Schumann and Moeng (1991a,b), and Moeng and Schumann (1991).

The existing bulk mass-flux models do not match the fluxes associated with the convective mass flux with those driven by ventilation at the surface and entrain-

* The National Center for Atmospheric Research is sponsored by the National Science Foundation.

Corresponding author address: Dr. David Randall, Department of Atmospheric Science, Colorado State University, Fort Collins, CO 80523.

ment at the top. Also, no existing bulk mass-flux model includes a physically based method to determine σ, the fractional area covered by rising motion. Finally, most of the existing bulk mass-flux models have retained the "well-mixed" assumption, with the notable exceptions of Betts (1973), Albrecht et al. (1979), and Wang and Albrecht (1990).

This paper addresses all three of these problems.

2. Convective mass-flux model

The basic framework of our model is shown in Fig. 1. The level just above the PBL top is denoted by subscript $B+$, while the earth's surface is denoted by $S-$. We define an infinitesimal "ventilation layer" just above the earth's surface and an infinitesimal "entrainment layer" just below the PBL top. These are indicated by stippling in Fig. 1. The ventilation layer is more conventionally known as the surface layer. The entrainment layer is the region within which the turbulent fluxes drop sharply from finite values to zero. Caughey et al. (1982) and Nicholls and Turton (1986) describe the entrainment layer as a thin region of weak organized vertical motions and vigorous small-scale mixing. The top of the ventilation layer will be denoted by subscript S, and the base of the entrainment layer by subscript B. The depth of the PBL (in terms of pressure) is denoted by δp_M.

The generic variable ψ will be used to represent a prognostic intensive scalar such as the dry static energy, the mixing ratio of water, or a velocity component. Area-averaged values of ψ are denoted by $\bar{\psi}$. The upward turbulent flux of ψ is denoted by F_ψ. The midlevel of the PBL is indicated by the dashed line in Fig. 1; it is representative of the interior of the PBL and will be denoted by subscript I.

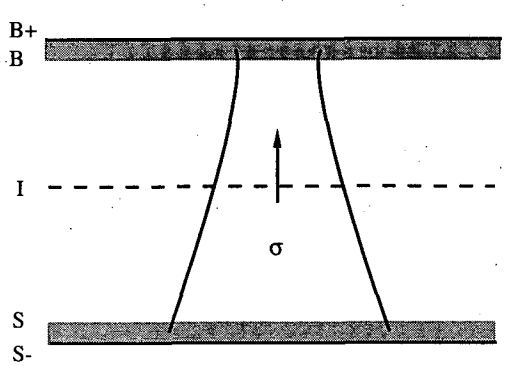

FIG. 1. Diagram illustrating the assumed structure of the PBL. The interior, which is represented by two layers, is bounded above by a thin entrainment layer and below by a thin ventilation layer. Convective circulations occur, with rising branches occupying fractional area σ. The ascending and descending branches have different thermodynamic soundings and, therefore, different cloud-base levels.

An entrainment mass flux E carries mass across the PBL top and is closely related to the turbulent fluxes at the base of the entrainment layer. Correspondingly, a ventilation mass flux V is associated with the surface fluxes; in conventional parlance, V is the product of the surface air density, the surface wind speed, and a transfer coefficient. The fluxes at the top of the ventilation layer are assumed to be approximately equal to those at the surface. As explained later, the model incorporates diagnostic balances for mass $\bar{\psi}$ and ψ'^2 for both the entrainment and ventilation layers. These layers are assumed to be thin enough so that these approximations are applicable.

Within the ventilation layer, the turbulent fluxes have to be carried by small eddies, since the organized vertical motions associated with the convective circulations must vanish there. Within the entrainment layer the organized vertical motions associated with the convective circulations become negligible. Since the turbulent fluxes vanish above the PBL top, however, it is not necessary to hypothesize that small-eddy fluxes are important in the entrainment layer. Nevertheless, the existence of small eddies within the entrainment layer is well known from observations (e.g., Rayment and Readings 1974).

As indicated in Fig. 1, we assume that the turbulent fluxes in the interior of the PBL are entirely due to the convective circulations, with rising branches covering fractional area σ and sinking branches covering fractional area $1 - \sigma$. Some authors (e.g., Greenhut and Khalsa 1982) have suggested a third, "environmental" domain in which the vertical motion is nearly zero. We are not willing to accept such a complication without strong evidence that it is really necessary. The results of Schumann and Moeng (1991a) suggest that it is not.

There have been numerous observations and numerical simulations yielding values of σ, based on various sampling methods. The methods used and results obtained are summarized in Table 1. Note that the various studies are based on data from several different PBL regimes and employ several different definitions of σ. They have yielded a variety of numerical values for σ. For example, Manton (1977), Coulman (1978), and Lenschow and Stephens (1978) have adopted definitions involving not only the vertical velocity fluctuations but also the thermodynamic fluctuations. In these three studies, σ is found to be considerably less than 0.5. All of the remaining studies have adopted definitions based only on the sign of the vertical velocity. Greenhut and Khalsa (1982) and Schumann and Moeng (1991a) define three domains: updrafts, downdrafts, and an environment. The updrafts consist of regions in which the vertical velocity exceeds a positive threshold. If we take the fractional area covered by updrafts to be σ, then Greenhut and Khalsa obtained $\sigma = 0.16$, by far the smallest value obtained in any of

TABLE 1. Summary of observations and simulations of the fractional area covered by rising motion in several studies. Here $\langle\ \rangle$ denotes the expected value.

Author	Source of data	Sampling method used to define "updraft"	Mean σ
Manton (1977)	Observations	$T > T_{th}$ such that $\langle w(T_{th})\rangle = 0$	0.42
Coulman (1978)	Observations	Similar to Manton (1977)	0.38
Lamb (1978)	LES results for clear PBL	Vertical velocity is positive	0.45
Greenhut and Khalsa (1982)	Observations	Vertical velocity exceeds a positive threshold. Three domains are defined: one for updrafts, one for downdrafts, and one for "environment."	0.16
Lenschow and Stephens (1982)	Observations	Moisture fluctuation is positive	0.25
Young (1988a)	Observations	Vertical velocity is positive	0.46
Nicholls (1989)	Observations of stratus-topped PBL over the North Sea	Vertical velocity is positive	0.70
Schumann and Moeng (1991a)	LES results	Vertical velocity exceeds a positive threshold. Three domains are defined: one for updrafts, one for downdrafts, and one for "environment."	0.35

the studies, while Schumann and Moeng obtained $\sigma = 0.35$. We note, however, that Schumann and Moeng concluded that little is to be gained by defining an environment for the updrafts and downdrafts.

The remaining three studies listed in Table 1 [i.e., those by Lamb (1978), Young (1988a), and Nicholls (1989)] adopted definitions of σ that are essentially the same as ours, namely, that σ is the fractional area covered by positive vertical velocity. The first two authors obtained values of σ equal to or slightly less than 0.5. Only the observations of Nicholls (1989), obtained by aircraft in stratocumulus clouds, show σ near 0.7. We conclude that σ is by no means a universal constant but that with the definition we have adopted here we should expect σ to be not too different from one-half under some conditions of interest.

Consider an arbitrary scalar ψ satisfying a conservation equation of the form

$$\frac{\partial}{\partial t}(\rho\psi) = -\nabla\cdot(\rho\mathbf{V}\psi) - \frac{\partial}{\partial z}(\rho w\psi) + S_\psi, \quad (2.1)$$

where ρ is the density, which is quasi constant in time and the horizontal, as in the usual anelastic approximation: $\mathbf{V}$ is the horizontal velocity vector; w is the vertical velocity; and S_ψ is the source of ψ per unit mass per unit time. The local time derivative and the ∇ operator are defined on constant height surfaces.

Area averages satisfy

$$\bar{\psi} = \psi_u\sigma + \psi_d(1-\sigma). \quad (2.2)$$

Here subscripts u and d denote upward and downward moving parcels, respectively. The fluxes associated with the convective circulations are given by

$$\begin{aligned} F_\psi = \rho\overline{w'\psi'} &= \rho[(w_u - \bar{w})(\psi_u - \bar{\psi})\sigma \\ &\quad + (w_d - \bar{w})(\psi_d - \bar{\psi})(1-\sigma)] \\ &= M_c(\psi_u - \psi_d), \end{aligned} \quad (2.3)$$

where

$$M_c \equiv \rho\sigma(1-\sigma)(w_u - w_d) \quad (2.4)$$

is the convective mass flux.

For later use, we note that the variance of ψ is given by

$$\begin{aligned} \overline{\psi'^2} &= \sigma(\psi_u - \bar{\psi})^2 + (1-\sigma)(\psi_d - \bar{\psi})^2 \\ &= \sigma(1-\sigma)(\psi_u - \psi_d)^2 \\ &= \sigma(1-\sigma)\left(\frac{F_\psi}{M_c}\right)^2, \end{aligned} \quad (2.5)$$

while the plume-scale variance transport can be written as

$$\begin{aligned} \rho\overline{w'\psi'\psi'} &= \rho[\sigma(w_u - \bar{w})(\psi_u - \bar{\psi})^2 \\ &\quad + (1-\sigma)(w_d - \bar{w})(\psi_d - \bar{\psi})^2] \\ &= \rho\sigma(1-\sigma)(1-2\sigma)(w_u - w_d)(\psi_u - \psi_d)^2 \\ &= (1-2\sigma)\frac{(F_\psi)^2}{M_c}. \end{aligned} \quad (2.6)$$

According to (2.6), $\rho\overline{w'\psi'\psi'}$ is positive (upward variance transport) if σ is less than 1/2 and negative (downward variance transport) if σ is greater than 1/2. For $\sigma = 1/2$ the variance transport vanishes. It follows that if the ventilation layer is exporting variance [production exceeds dissipation, and $(\rho\overline{w'\psi'\psi'})_S$ is upward], then σ_S must be less than 1/2; this would normally be the case for a clear convective PBL driven by surface heating. Similarly, if the entrainment layer is exporting variance [production exceeds dissipation, and $(\rho\overline{w'\psi'\psi'})_B$ is downward], then σ_B must be greater than 1/2.

Now and from time to time throughout the rest of this paper, we investigate the consistency of our simple model with LES results obtained by C.-H. Moeng. These results are similar to the stratocumulus simulations of Moeng (1986) except that the domain size was doubled to 5 km × 5 km × 1 km and 80^3 grid points were used. The vertical resolution was 12.5 m. The horizontal resolution was 62.5 m. We have used six LES history records, spaced 250 simulated seconds apart. These same LES results were analyzed by Schumann and Moeng (1991a; their "STBL" case).

Figure 2 shows $\bar{h}/c_p$ and $\bar{q}_t$ plotted as functions of height. Here $h \equiv s_v - Lq_l$, c_p is the specific heat of air at constant pressure, and q_t is the total mixing ratio (vapor plus liquid). We use s_v to denote the virtual dry static energy and q_l to denote the liquid water mixing ratio. The figure shows averages over the six LES history records. The expected well-mixed interior and near-discontinuities at the top and bottom of the PBL are readily apparent.

We propose a method to determine σ and M_c, based entirely on the vertical velocity statistics and suggested by the analysis of Moeng and Rotunno (1990). The idea is to use (2.2), (2.5), and (2.6) with $\psi = w$ and to solve these three equations for the three unknowns σ, w_u, and w_d. The convective mass flux can then be evaluated using (2.4). We find that

$$\sigma = \frac{1}{2} - \frac{S_w}{2\sqrt{4 + S_w^2}}, \tag{2.7}$$

where

$$S_w \equiv \frac{\overline{w'^3}}{(\overline{w'^2})^{3/2}} \tag{2.8}$$

is the skewness of the vertical velocity. A similar result was obtained by Wyngaard and Brost (1984). According to (2.7), σ is less than 1/2 when the skewness is positive and greater than 1/2 when the skewness is negative. The form of (2.7) guarantees that $0 < \sigma < 1$. The convective mass flux satisfies

$$M_c = \frac{\rho\sqrt{\overline{w'^2}}}{\sqrt{4 + S_w^2}}. \tag{2.9}$$

One advantage of this approach is that it guarantees consistency between the mass flux and the variance of the vertical velocity, within the context of the mass-flux model. A second advantage is that it can be used to determine σ and M_c in a higher-order closure model. Of course, we cannot use this method to determine σ and M_c in a bulk mass-flux model because such a model does not provide the needed input data; for example, S_w is not available. Later, in section 4, we present a method that can be used to determine σ and M_c in a bulk mass-flux model.

Figure 3a shows the profiles of w_u and w_d obtained by the method described above and by directly sam-

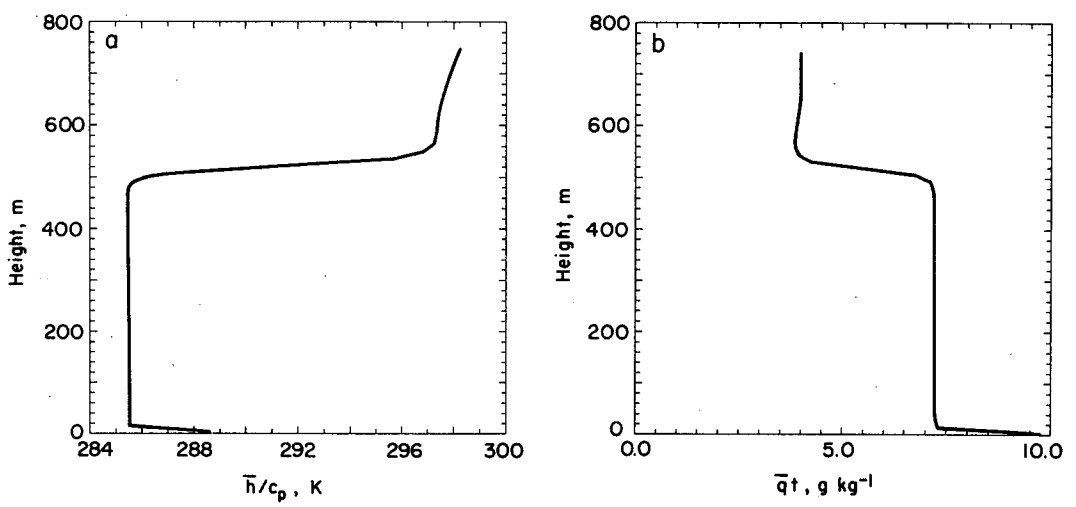

FIG. 2. The vertical profiles of $\bar{h}$ and $\bar{q}_t$, plotted as functions of height.

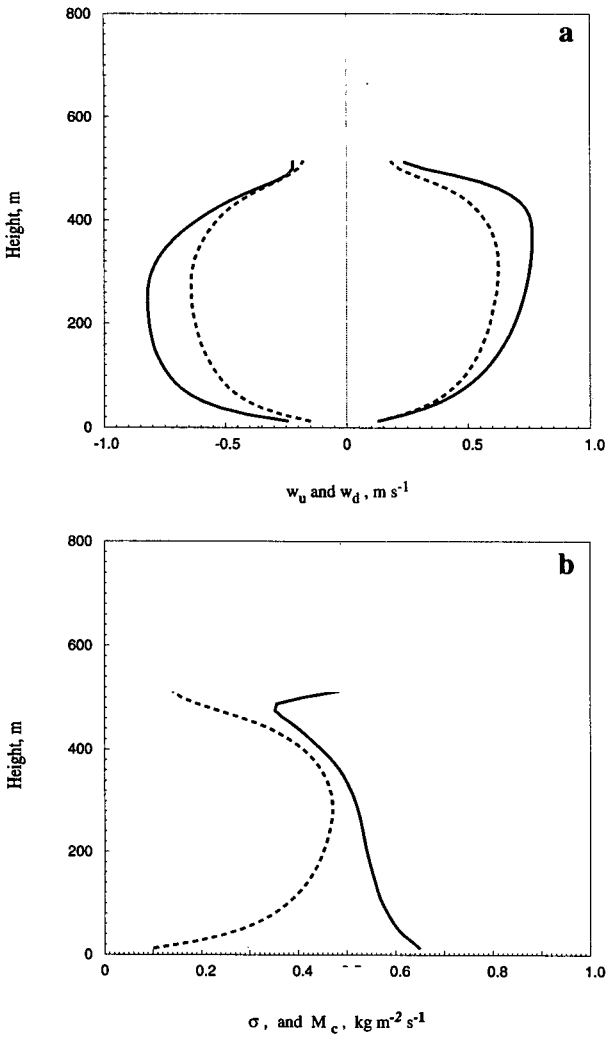

FIG. 3. (a) The vertical profiles of w_u and w_d obtained by the method described in section 2 (solid curves) and also by directly sampling the LES results (dashed curves). (b) The vertical profiles of σ (solid curve) and M_c (dashed curve), plotted as functions of height normalized by the PBL depth. Values are not plotted above the PBL top since σ and M_c have little meaning there.

pling the LES results. The profiles are quite similar, but the method proposed here systematically overestimates the magnitudes of w_u and w_d. Figure 3b shows the profiles of σ and M_c, obtained from the LES results by the method described in the preceding paragraph. Although σ is close to 0.5 at all levels, it decreases noticeably upward through most of the PBL's depth, from about 0.6 near the surface to about 0.4 slightly below the PBL top. This is consistent with the analysis of Moeng and Rotunno (1990). The convective mass flux has a roughly parabolic profile, with a maximum slightly above the midlevel of the PBL, and much smaller values near the surface and the PBL top. The maximum value of M_c is about 0.45 kg m^{-2} s^{-1}.

Using (2.2) and (2.3), we can evaluate ψ_u and ψ_d as follows:

$$\psi_u = \bar{\psi} + \frac{1-\sigma}{M_c} F_\psi, \tag{2.10}$$

$$\psi_d = \bar{\psi} - \frac{\sigma}{M_c} F_\psi. \tag{2.11}$$

The values of ψ_u and ψ_d obtained directly by conditional sampling (based on the sign of the vertical velocity) are slightly different from those obtained from the fluxes using (2.10)–(2.11). This is shown in Fig. 4a for h/c_p and in Fig. 4b for q_t. In these figures the solid

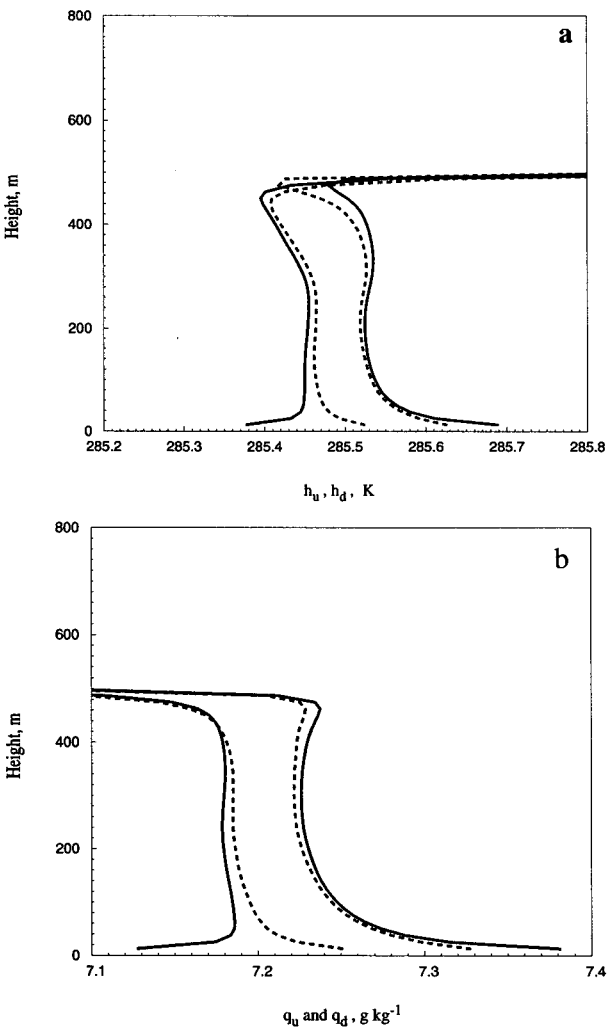

FIG. 4. Profiles of ψ_u and ψ_d calculated directly by conditional sampling (based on the sign of the vertical velocity) and from the fluxes using (2.10)–(2.11). (a) for h/c_p; (b) for q_t. The solid lines show the updraft and downdraft properties obtained from (2.10) and (2.11), and the dashed lines show the corresponding values based on conditional sampling.

lines show the updraft and downdraft properties obtained from (2.10)–(2.11), and the dashed lines show the corresponding values based on conditional sampling. The updrafts are "warm" and "wet," and the downdrafts are "cold" and "dry." To give the correct fluxes, (2.10)–(2.11) make the updrafts warmer and wetter and the downdrafts colder and drier than the corresponding updraft and downdraft properties obtained by conditional sampling (cf. Young 1988a; Wang and Albrecht 1990; Schumann and Moeng 1991a). The discrepancies are fairly small, however, compared to the differences between the updraft and downdraft properties. These discrepancies are due to the "top-hat" profiles assumed in the convective mass-flux model. In a sense, the mass circulation of the convective mass-flux model produces fluxes less efficiently than the more realistic simulation produced through LES. In the remainder of this paper we use ψ_u and ψ_d as determined from (2.10)–(2.11).

3. Matching the fluxes

The surface fluxes are assumed to satisfy the usual bulk aerodynamic formula,

$$(F_\psi)_S = V(\bar{\psi}_{S-} - \bar{\psi}_S), \tag{3.1}$$

where V is the "ventilation mass flux," which is usually written as the product of surface wind speed, a transfer coefficient, and the surface air density.

We assume that the fluxes at the top of the ventilation layer are entirely due to the convective circulations and that the small-eddy fluxes are negligible there. Using this assumption with (2.3) and (3.1), and also using our assumption that the ventilation layer is thin, we can write

$$V(\bar{\psi}_{S-} - \bar{\psi}_S) = M_{c,S}(\psi_u - \psi_d)_S. \tag{3.2}$$

This condition implies a consistency between the fluxes obtained from the bulk formula and those determined from the mass-flux model. Wang and Albrecht (1990) did not impose (3.2) or the corresponding condition at the PBL top (discussed later).

At level S the parcels rising away from the lower boundary must be "charged" with the properties of the boundary. We cannot assume, however, that the properties of the updrafts at level S are *the same* as those of the boundary, because there can be very strong gradients across the ventilation layer. The small eddies of the ventilation layer rapidly dilute air that has been in contact with the boundary by mixing it with air that has recently descended from the interior of the PBL. As a result, $|\bar{\psi}_{S-} - \bar{\psi}_S| \gg |(\psi_u - \psi_d)_S|$; from (3.2) this implies that $M_{c,S} \gg V$. In order to take this into account we introduce a nondimensional parameter χ_V such that

$$(\psi_u)_S - \bar{\psi}_S = \chi_V(\bar{\psi}_{S-} - \bar{\psi}_S); \tag{3.3}$$

in case $\chi_V = 1$, we get $(\psi_u)_S = \bar{\psi}_{S-}$. Smaller values of χ_V indicate stronger mixing by the small eddies of the ventilation layer. We expect $0 < \chi_V \ll 1$. By combining (2.2), (3.2), and (3.3), we find that

$$\chi_V G_V = 1 - \sigma_S, \tag{3.4}$$

where $G_V \equiv M_{c,S}/V$. This is a "continuity equation" for the eddies, expressing a relationship between the convective mass flux and the ventilation mass flux.

In the preceding discussion it has been tacitly assumed that χ_V is independent of ψ, that is, that a single "mixing" parameter χ_V satisfies (3.3) whether ψ is moist static energy, total water mixing ratio, or some other intensive scalar. This assumption is supported by (3.4); if $M_{c,S}$, V, and σ_S are all independent of ψ, then χ_V must also be independent of ψ. Such independence suggests that χ_V is a useful concept.

We now apply a similar analysis to the entrainment layer. The assumption that it is thin yields the familiar "jump" relation between $(F_\psi)_B$ and the entrainment rate:

$$(F_\psi)_B = -E(\bar{\psi}_{B+} - \bar{\psi}_B) - \int_{z_B}^{z_{B+}} \overline{S_\psi} dz. \tag{3.5}$$

Here E is the rate at which mass is entrained across the PBL top. In (3.5) we follow Lilly (1968) by keeping the S_ψ term, which represents a possible concentrated entrainment-layer "source" of ψ (e.g., due to radiation). We now assume that the fluxes at the base of the entrainment layer are entirely due to the convective circulations and that the small-eddy fluxes are negligible. Then, by comparing (2.3) and (3.5) and using (2.2), we obtain

$$M_{c,B}(\psi_d - \bar{\psi})_B = E\sigma_B(\bar{\psi}_{B+} - \bar{\psi}_B) + \sigma_B \int_{z_B}^{z_{B+}} \overline{S_\psi} dz. \tag{3.6}$$

At this point, we introduce a mixing parameter χ_E by analogy with (3.3). To allow for the effects of the concentrated source, however, we include an additional term:

$$(\psi_d - \bar{\psi})_B = \chi_E(\bar{\psi}_{B+} - \bar{\psi}_B) + \lambda \int_{z_B}^{z_{B+}} \overline{S_\psi} dz. \tag{3.7}$$

Here λ is a coefficient that is determined later. According to (3.7), the properties of the descending air at level B are related to those of the free atmosphere just above the PBL top, as modified by small-eddy mixing and the effects of any concentrated source within the entrainment zone. Since there is a sharp gradient of ψ across the entrainment layer, we expect $0 < \chi_E \ll 1$.

The mixing parameter χ_E is closely related to the parameter χ discussed by Siems et al. (1989) (see also Albrecht et al. 1985; Nicholls and Turton 1986). We

can interpret χ_E as the value of χ associated with the downdraft air at level B. Further discussion is given later in this section.

Comparing (3.6) with (3.7), we find that

$$(-M_{c,B}\chi_E + E\sigma_B)(\bar{\psi}_{B+} - \bar{\psi}_B) + (-M_{c,B}\lambda + \sigma_B)\int_{z_B}^{z_{B+}} \overline{S_\psi} dz = 0. \quad (3.8)$$

In case the source term of (3.8) vanishes, we obtain

$$\chi_E G_E = \sigma_B, \quad (3.9)$$

where $G_E \equiv M_{c,B}/E$. This relationship does not involve ψ; it must therefore apply for *all* ψ. To ensure that (3.9) will be satisfied even when the source term of (3.8) is not zero, we must choose

$$\lambda = \sigma_B/M_{c,B}. \quad (3.10)$$

We can interpret (3.9) as another "continuity equation," analogous to (3.4). Again, we have tacitly assumed that χ_E is independent of the species under consideration. This assumption is consistent with (3.9), since $M_{c,B}$, E, and σ_B are independent of species. We can use (3.9) to eliminate $M_{c,B}$ in (3.6), or alternatively, use (3.10) to eliminate λ in (3.7); either way, the result is

$$(\psi_d)_B = \chi_E\overline{\psi_{B+}} + (1 - \chi_E)\bar{\psi}_B + \frac{\chi_E}{E}\int_{z_B}^{z_{B+}} \overline{S_\psi} dz. \quad (3.11)$$

According to (3.11), the descending air at level B has the properties of the free atmosphere, except as modified by mixing (when $\chi_E < 1$) and by the concentrated source. Caughey et al. (1982) and Nicholls (1989) have reported observations of cool downdrafts in the upper portions of stratocumulus cloud sheets. They concluded that the sinking air had been radiatively cooled near the cloud top. Such effects are represented by the S_ψ term of (3.11).

This term is inversely proportional to E, which means that radiative cooling in the entrainment layer can produce negatively buoyant parcels most effectively if the entrainment rate is slow. This suggests that entrainment driven by radiative cooling near cloud top tends to be self-limiting.

According to (3.4), ventilation-layer dilution becomes more effective (in other words, χ_V decreases) as the convective mass flux increases relative to $V(1 - \sigma_S)$. The ventilation mass flux times the fractional area covered by the incoming downdrafts is a measure of the rate at which the updrafts leaving the ventilation layer can be supplied with air that has been charged with surface properties, and the convective mass flux is a measure of the rate at which this air is removed from the surface layer. The stronger the convective mass flux becomes, the less effectively ventilation-layer air can be charged with surface properties before it is carried away into the interior of the PBL. A similar interpretation can be given for (3.9).

If we combine (3.4) and (3.9) and assume that σ is independent of height through the depth of the PBL so that $\sigma_S = \sigma_B$, we find that

$$\sigma = \frac{1}{1 + \chi_V G_V/\chi_E G_E}. \quad (3.12)$$

Suppose that M_c is also independent of height so that $M_{c,S} = M_{c,B}$. If we substitute (3.12) back into either (3.4) or (3.9) and use the definitions of G_V and G_E, we obtain

$$M_c = \frac{(E/\chi_E)(V/\chi_V)}{(E/\chi_E) + (V/\chi_V)}. \quad (3.13)$$

With the assumption that M_c is independent of height, (3.12) can be rewritten as

$$\sigma = 1\Big/\left(1 + \frac{E}{V}\frac{\chi_V}{\chi_E}\right). \quad (3.14)$$

Of course, bulk PBL models normally include parameterizations for V and E. If we have a parameterization of χ_V/χ_E, then (3.14) can be used to determine σ. Note that the *forms* of (3.12) and (3.14) ensure that $0 < \sigma < 1$. We use both (3.13) and (3.14) later in this paper.

The profiles of σ and M_c shown in Fig. 3 are not independent of height. Nevertheless, the assumption that these two parameters are vertically uniform is of interest as a particularly simple special case.

Now we test the main conclusions of this section, using the LES results.

First we have to identify levels $S-$, S, B, and $B+$ based on the LES output. In this we are guided not only by the mean structures but also by the turbulence results, since we have defined the ventilation and entrainment layers in terms of the relative importance of small-eddy fluxes. Figure 5 shows the mean structure of the total moisture q_t (g kg^{-1}, solid line) and the ratio of the subgrid moisture flux to the total moisture flux. The ratio becomes appreciable only near the top and bottom of the PBL. We identify the entrainment and ventilation layers as those regions within which the ratio exceeds 0.1. We have also taken into account the mean structure. The entrainment and ventilation layers that we have identified are indicated in Fig. 5. The height of level $S-$ is zero (the surface), while level S is at 62.5 m, level B is at 475 m, and level $B+$ is at 537.5 m. The average cloud top is near 504 m. Since the vertical grid spacing of the LES model is 12.5 m, there are four model layers inside the ventilation layer and four more inside the entrainment layer.

Averaging over six LES history records, we obtain

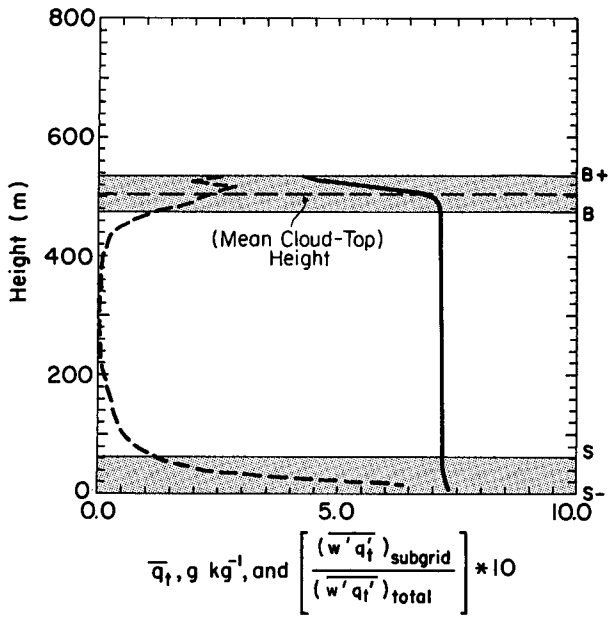

FIG. 5. For the LES results, the ratio of the subgrid-scale moisture flux to the total flux. The ventilation and entrainment layers are indicated by stippling.

the following numerical values for the mean-state variables:

$$\overline{h_{B+}}/c_p = 295.73 \text{ K},$$
$$\overline{h_B}/c_p = 285.45 \text{ K},$$
$$\overline{(q_t)}_{B+} = 4.22 \text{ g kg}^{-1},$$
$$\overline{(q_t)}_B = 7.18 \text{ g kg}^{-1},$$
$$\overline{h_S}/c_p = 285.51 \text{ K},$$
$$\overline{h_{S-}}/c_p = 288.67 \text{ K},$$
$$\overline{(q_t)}_S = 7.23 \text{ g kg}^{-1},$$
$$\overline{(q_t)}_{S-} = 9.80 \text{ g kg}^{-1}.$$

These values are indicated in Fig. 2.

We have evaluated the ventilation mass flux from the LES results, as the ratio of the surface flux of h or q_t to the surface–air difference in the same quantity, as indicated in (3.1). Averaging over six LES history records, the ventilation mass flux based on h is 1.04×10^{-2} kg m^{-2} s^{-1}, while that based on q_t is 0.965×10^{-2} kg m^{-2} s^{-1}. We estimate, therefore, that the correct value of V is about 1.0×10^{-2} kg m^{-2} s^{-1}.

Table 2 gives the entrainment mass flux E as evaluated from the LES data by the following methods.

Method HA:

$$E_h = \frac{\Delta R + (F_h)_{B+} - (F_h)_B}{\overline{\Delta h}}$$

Method HB:

$$E_h = \frac{\Delta R - (F_h)_B}{\overline{\Delta h}}$$

Method QA:

$$E_q = \frac{(F_{qt})_{B+} - (F_{qt})_B}{\overline{\Delta q_t}}$$

Method QB:

$$E_q = \frac{-(F_q)_B}{\overline{\Delta q_t}}$$

Method Z:

$$E = \rho \frac{dz_T}{dt} - \rho \bar{w}_B.$$

Here z_T is the cloud-top height. Methods HA and QA include the small contributions from the fluxes at level $B+$, and so are a priori more reliable than methods HB and QB. Our results indicate that the effect of fluxes at level $B+$ on the estimated entrainment rate amounts to about 20%. Method Z does not give a reliable value for the entrainment rate because of uncertainties in determining the values of z_T and especially its time change; we have shown only the average value based on the total length of the record available to us. From the results given in Table 2, we conclude that the correct value of E is about 0.82×10^{-2} kg m^{-2} s^{-1}. This corresponds to an "entrainment velocity" of about 25 m h^{-1} or about 600 m day^{-1}, which is in line with observations (e.g., Nicholls and Turton 1986). Note that E and V are quite comparable in magnitude.

We have argued that χ_V and χ_E are independent of species. Do the LES results support this? Substituting (2.10) and (2.11) into (3.3) and (3.6), and using (3.10), we obtain expressions for χ_V and χ_E:

$$\chi_V = \left(\frac{1 - \sigma_S}{M_{cS}}\right)\left[\frac{(F_\psi)_S}{\bar{\psi}_{S-} - \bar{\psi}_S}\right], \tag{3.15}$$

TABLE 2. The LES entrainment mass flux in 10^{-2} kg m^{-2} s^{-1}, as determined by methods HA, HB, QA, QB, and Z. See text for explanation of the methods.

	History record number						
	1	2	3	4	5	6	Average
HA	0.803	0.768	0.816	0.814	0.797	0.841	0.806
HB	0.660	0.639	0.666	0.691	0.741	0.767	0.694
QA	0.819	0.786	0.859	0.835	0.853	0.833	0.831
QB	0.633	0.625	0.670	0.671	0.760	0.733	0.682
Z							0.656

$$\chi_E = -\left(\frac{\sigma_B}{M_{c,B}}\right)\left[\frac{(F_\psi)_B + \int_{z_B}^{z_{B+}} \bar{S}_\psi dz}{\bar{\psi}_{B+} - \bar{\psi}_B}\right]. \quad (3.16)$$

For $\psi = q_t$, we have $S_\psi = 0$, while for $\psi = h$ we have

$$-\int_{z_B}^{z_{B+}} \bar{S}_\psi dz = \Delta\bar{R} = -\int_{z_B}^{z_{B+}} \overline{\rho c_p \left(\frac{\partial T}{\partial t}\right)_{\text{RAD}}} dz, \quad (3.17)$$

where $(\partial T/\partial t)_{\text{RAD}}$ is the heating rate due to longwave radiation.

Using the methods of section 2, we have evaluated σ and the convective mass fluxes at levels B and S. The results, averaged over the six history records, are $\sigma_S = 0.595$, $\sigma_B = 0.352$, $M_{c,S} = 0.316$ kg m^{-2} s^{-1}, and $M_{c,B} = 0.235$ kg m^{-2} s^{-1}. From the mass fluxes, we obtain $G_V = 31.56$ and $G_E = 28.66$. We have also evaluated $\overline{\Delta R}$ by using (3.17). The result is $\overline{\Delta R} = 82.1$ W m^{-2}. In a similar way, we have determined that the radiative flux "jump" across the ventilation layer is a warming of 2.2 W m^{-2}.

We have also determined χ_V and χ_E using each of the six LES history records. For this purpose, we used (3.3) and (3.7), with the numerical values of ψ_u, ψ_d, and $\bar{\psi}$ given earlier. The results are given in Table 3. The χ_E obtained for $\psi = h$ and $\psi = q_t$ agree very well. Note that $\chi_{V,h}$ is generally a little bit larger than $\chi_{V,q}$. If we include the small radiative flux jump across the ventilation layer, we find that the two χ_V agree as well as the two χ_E do. On the basis of these results, we conclude that $\chi_V = 1.22 \times 10^{-2}$ and that $\chi_E = 1.02 \times 10^{-2}$. The good agreement between the values of χ obtained with h and q_t supports our assertion that χ_V and χ_E are independent of species. As expected, both χ_V and χ_E are small compared to unity. Their numerical values are quite similar.

Since we have chosen V and E so that (3.1) and (3.5) are satisfied, the good results presented above for χ_V and χ_E ensure that (3.4) and (3.9) will be satisfied. Substituting our "best estimates" of E, V, χ_V, and χ_E into (3.14), we find that the effective height-independent value of σ is 0.505, in reasonably good agreement with the LES results shown in Fig. 3.

Using the numerical values given above for E, V, χ_E, and χ_V, we find from (3.13) that the effective height-independent value of M_c is 0.406 kg m^{-2} s^{-1}. This is slightly larger than the value of $M_{c,S}$ obtained directly from the LES results, and is substantially larger than the value of $M_{c,B}$. It is fairly close to the maximum value of M_c shown in Fig. 3.

Before leaving this section, we offer an alternative interpretation of χ_E. The air descending at level B is a mixture of updraft air that has passed through the entrainment layer and newly entrained air from level $B+$. Let f be the fraction of air from level $B+$; that is,

$$(\psi_d)_B = (\psi_u)_B(1 - f) + f\overline{\psi_{B+}}. \quad (3.18)$$

For simplicity we have assumed no concentrated sources or sinks. Note, however, that this assumption does not alter the result below. Comparing (3.18) with (3.7), we find that

$$f = \frac{\chi_E}{\chi_E + \sigma_B(1 - \chi_E)}. \quad (3.19)$$

Substituting the numerical values of σ and χ_E from above, we obtain $f \approx 0.028$. This means that, for the case studied here, about 3% of the air descending at level B has just been entrained; the remainder is "recycled" updraft air.

Appendix A presents an analysis of the budgets of $\overline{\psi'^2}$ for the entrainment and ventilation layers.

4. The convective mass flux and the turbulence kinetic energy

In this section, we present methods to determine σ and M_c inside the convective mass-flux model, using the turbulence kinetic energy (TKE) and the entrainment and ventilation mass fluxes as inputs.

Obviously, there has to be a close connection between the convective mass flux and the turbulence kinetic energy. Let a_3 be the fraction of the vertically integrated TKE that resides in the vertical component of the motion. We can write

$$a_3 e_M \int_{z_{S-}}^{z_{B+}} \rho dz = \frac{1}{2}\int_{z_{S-}}^{z_{B+}} \rho\overline{w'^2} dz. \quad (4.1)$$

TABLE 3. Values of χ_V and χ_E determined from the LES results by various methods. Subscript q indicates that we have used $\psi = q_t$, while subscript h indicates that we have used $\psi = h$. In the case of $\chi'_{V,h}$ we have taken into account the weak radiative forcing of the ventilation layer. This slightly reduces the values of $\chi_{V,h}$, bringing them into better overall agreement with those of $\chi_{V,q}$.

	History record number						
	1	2	3	4	5	6	Average
$\chi_{V,q}$	0.0124	0.0124	0.0130	0.0121	0.0125	0.0119	0.0124
$\chi_{V,h}$	0.0126	0.0137	0.0140	0.0130	0.0140	0.0127	0.0133
$\chi_{E,q}$	0.0097	0.0104	0.0101	0.0094	0.0109	0.0106	0.0101
$\chi_{E,h}$	0.0101	0.0106	0.0101	0.0097	0.0107	0.0110	0.0104
$\chi'_{V,h}$	0.0113	0.0124	0.0128	0.0117	0.0127	0.0114	0.0121

Here e_M is the vertically averaged TKE per unit mass. If the TKE is equipartitioned among the three convective velocity components, then $a_3 = 1/3$. Using the LES results and considering only the resolved-scale motions in the region $z_{S-} \leq z \leq z_{B+}$, we find that $e_M = 0.712\ \text{m}^2\ \text{s}^{-2}$ and $a_3 = 0.281$.

Using (2.3), we can express $\overline{w'^2}$ in terms of the difference in vertical velocity between the updrafts and the downdrafts. Next, (2.4) can be used to rewrite this difference in terms of the convective mass flux, giving

$$\overline{w'^2} = \frac{M_c^2}{\rho^2 \sigma(1-\sigma)}. \tag{4.2}$$

Because of the way we have determined σ and M_c from the LES results (see section 2), (4.2) has to be exactly satisfied when $\overline{w'^2}$ is evaluated from the LES. By substitution from (4.2), (4.1) can be rewritten as

$$a_3 e_M \int_{z_{S-}}^{z_{B+}} \rho dz = \frac{1}{2} \int_{z_{S-}}^{z_{B+}} \frac{M_c^2}{\rho\sigma(1-\sigma)}\, dz. \tag{4.3}$$

If σ and M_c are independent of height, then (4.3) reduces to

$$M_c = \left(\frac{2a_3\sigma(1-\sigma)e_M \int_{z_{S-}}^{z_{B+}} \rho dz}{\int_{z_{S-}}^{z_{B+}} \frac{1}{\rho}\, dz} \right)^{1/2}. \tag{4.4}$$

The integrals in (4.4) are easily evaluated for a given sounding. If we consider the density of the air to be approximately constant with height in the PBL, then (4.4) can be simplified to

$$M_c = \rho_M \sqrt{2a_3\sigma(1-\sigma)e_M}. \tag{4.5}$$

Appendix B gives a method to predict e_M in a bulk boundary-layer model. Then (4.5) can be used to evaluate M_c, provided that σ is known.

From the LES results, we have already found, in section 3, that the effective height-independent values of M_c and σ are 0.406 kg m^{-2} s^{-1} and 0.505, respectively. Substituting numerical values into the rhs of (4.5), we obtain $M_c = 0.383$ kg m^{-2} s^{-1}. This is in fair agreement with the value just mentioned, and seems reasonable in view of the LES results shown in Fig. 3.

By equating (4.5) and (3.13), and using (3.14), we can derive a constraint on the product $\chi_V \chi_E$; that is,

$$\chi_V \chi_E = \frac{EV}{2a_3 \rho_M^2 e_M}. \tag{4.6}$$

Substituting numerical values on the rhs of (4.6) gives $\chi_V \chi_E = 1.40 \times 10^{-4}$, which should be compared with the value inferred in section 3; that is, $\chi_V \chi_E = (1.22 \times 10^{-2}) \times (1.02 \times 10^{-2}) = 1.24 \times 10^{-4}$.

Alternatively, we can set the lhs of (4.5) to 0.406 kg m^{-2} s^{-1}, which is the value obtained in section 3, and solve (4.5) for a_3. This gives $a_3 = 0.316$, which is slightly larger than the value obtained directly from the LES results mentioned before. This small discrepancy in a_3 comes from our assumption that both σ and M_c are independent of height. If $a_3 = 0.316$ is used in (4.6), we are guaranteed to obtain the same value of $\chi_V \chi_E$ that we reported in section 3. Of course, given a method to determine χ_E and χ_V, we could use (4.6) to solve for a_3.

Our plan is to parameterize χ_E and χ_V. The parameterization must be consistent with (4.6). Note that the denominator on the rhs of (4.6) contains only quantities that characterize the PBL *as a whole,* rather than the entrainment or ventilation layers. We expect E and V to appear symmetrically in the expressions for χ_E and χ_V. The form of (4.6) thus suggests the following two alternative possibilities for χ_E and χ_V:

$$\chi_V = \frac{V}{\rho_M \sqrt{2a_3 e_M}}, \quad \chi_E = \frac{E}{\rho_M \sqrt{2a_3 e_M}}; \tag{4.7a}$$

or

$$\chi_V = \chi_E = \left(\frac{EV}{2a_3 \rho_M^2 e_M} \right)^{1/2}. \tag{4.7b}$$

Obviously, neither (4.7a) nor (4.7b) follows rigorously from (4.6); these are just two particularly plausible possibilities. A possible motivation for (4.7a) is that it pairs V with χ_V and E with χ_E, thus keeping ventilation-layer quantities together and entrainment-layer quantities together. A motivation for (4.7b) is that the product EV is, in a sense, characteristic of the PBL as a whole, so that it can plausibly appear symmetrically in the expressions for χ_E and χ_V.

Substituting the previously mentioned numerical values for the quantities on the rhs of (4.7a), we obtain $\chi_V = 1.31 \times 10^{-2}$ and $\chi_E = 1.07 \times 10^{-2}$. Similarly, (4.7b) gives $\chi_V = \chi_E = 1.18 \times 10^{-2}$. These values are reasonably close to those deduced from the LES results in section 2, that is, $\chi_V = 1.22 \times 10^{-2}$ and $\chi_E = 1.02 \times 10^{-2}$.

We can now substitute (4.7a) or (4.7b) back into (3.14) to obtain an expression for σ. From (4.7a) we obtain

$$\sigma = \frac{1}{2}, \tag{4.8a}$$

and from (4.7b)

$$\sigma = \frac{1}{1 + E/V}. \tag{4.8b}$$

Since E and V are practically equal in the LES results under discussion here, (4.8a) and (4.8b) give essentially the same numerical value for σ, and both are reasonably consistent with the LES results presented in section 3, which gave σ close to 1/2. It would be useful to have

observations or LES results for which E and V differed appreciably; if σ was also known, this would allow us to choose between (4.8a) and (4.8b).

5. Interiors

Up to this point we have discussed only the ventilation and entrainment layers. Now it is time to consider the interior of the PBL. The purpose of this section is to show how the well-mixed assumption can be relaxed by using a simple second-order closure, within the context of our bulk mass-flux model.

We assume that the variance budget of the PBL's interior satisfies

$$\frac{\partial}{\partial t}\overline{\psi'^2} = -2\frac{F_\psi}{\rho}\frac{\partial\bar{\psi}}{\partial z} - \frac{1}{\rho}\frac{\partial}{\partial z}(\rho\overline{w'\psi'\psi'}) - 2\epsilon_\psi. \quad (5.1)$$

Advection by the mean flow has been neglected, and we have assumed for simplicity that ψ is a conservative variable. (This assumption is not necessary and can easily be relaxed.) We now model each term of (5.1), following the methods introduced earlier. The variance itself is replaced by (2.5). The triple correlation in the transport term is replaced by (2.6). The dissipation is modeled by

$$\epsilon_\psi = \frac{\overline{\psi'^2}}{\tau_{\text{dis}}} = \frac{\sigma(1-\sigma)}{\tau_{\text{dis}}}\left(\frac{F_\psi}{M_c}\right)^2, \quad (5.2)$$

where τ_{dis} is a dissipation scale whose functional dependence on σ will be discussed later. With the assumptions that σ and M_c are independent of height, we find that

$$\frac{\partial}{\partial t}\left[\sigma(1-\sigma)\left(\frac{F_\psi}{M_c}\right)^2\right] = -2\frac{F_\psi}{\rho}\frac{\partial\bar{\psi}}{\partial z} - \frac{M_c(1-2\sigma)}{\sigma(1-\sigma)}\frac{1}{\rho}\frac{\partial}{\partial z}\left[\sigma(1-\sigma)\left(\frac{F_\psi}{M_c}\right)^2\right] - \frac{2\sigma(1-\sigma)}{\tau_{\text{dis}}}\left(\frac{F_\psi}{M_c}\right)^2. \quad (5.3)$$

It is interesting to consider the equilibrium ($\partial/\partial t = 0$) solutions of (5.3) for two limiting cases. First, suppose that $\sigma = 1/2$ so that the middle term (the transport term) of (5.3) drops out. Then we get

$$F_\psi = -\frac{M_c^2\tau_{\text{dis}}}{\sigma(1-\sigma)}\frac{1}{\rho}\frac{\partial\bar{\psi}}{\partial z}. \quad (5.4)$$

This is a downgradient diffusion formula.

Next, suppose that $\sigma \ll 1$, as in the case of cumulus convection. Then (5.3) reduces to

$$\frac{\partial F_\psi}{\partial z} = -M_c\frac{\partial\bar{\psi}}{\partial z}. \quad (5.5)$$

This is the "compensating subsidence" formula that has become familiar in cumulus parameterization theories. (The "detrainment" terms that appear in cumulus parameterizations can be included here too by relaxing our simplifying assumption that M_c is independent of height.)

In short, (5.3) includes both downgradient mixing and "compensating subsidence" as special cases.

Figure 6 shows the dissipation time scale obtained from the LES results, as a function of height, determined by using

$$\tau_{\text{dis}} = \frac{\overline{\psi'^2}}{\epsilon_\psi}, \quad (5.6)$$

for both h (solid line) and q_t (dashed line). Near the midlevel of the PBL, τ_{dis} is on the order of 1000 sec. It is considerably shorter near the surface and the PBL top. This might be because the resolved-scale variances are small near the edges of the PBL, or it might be because dissipation is actually more effective in those regions where small eddies are dominant. We use a single, height-independent value of τ_{dis} in our model. Further discussion of τ_{dis} is given later.

We can use these results in either of two ways, both of which allow us to relax the well-mixed assumption. On one hand, the equilibrium solution of (5.3) gives a constraint on $\partial\bar{\psi}/\partial z$ similar to that proposed by Wyngaard and Brost (1984). In fact, one way to proceed from here would be to adopt the formulas for $\partial\bar{\psi}/\partial z$ and F_ψ proposed by Wyngaard and Brost [e.g., their Eq. (46)], and to force consistency with our model. This approach would yield constraints on σ and M_c.

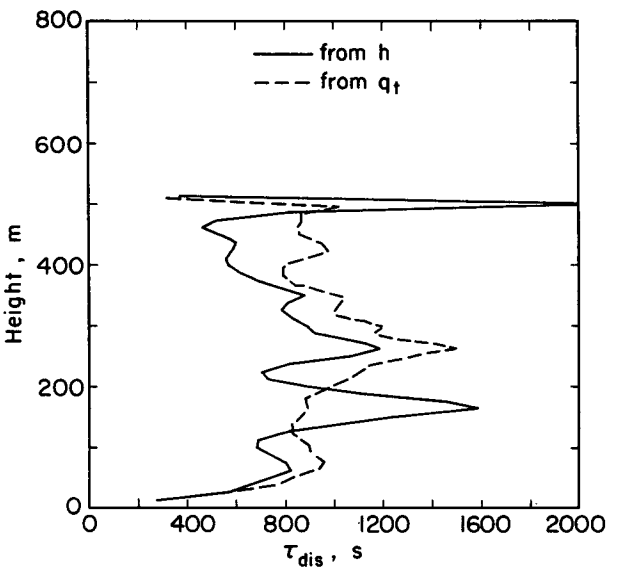

FIG. 6. Vertical profiles of τ_{dis}, as determined from the LES results for dissipation of h (solid line) and q_t (dashed line).

The other possible application of (5.3) is as follows. Note that (5.3) is hyperbolic; only the first derivative with respect to z of $\sigma(1-\sigma)(F_\psi/M)^2$ appears, and it is multiplied by the "velocity" $M_c(1-2\sigma)/[\rho\sigma(1-\sigma)]$. This velocity is upward (positive) if $\sigma < 1/2$ and downward (negative) if $\sigma > 1/2$. It follows that the single boundary condition on $\sigma(1-\sigma)(F_\psi/M_c)^2$ must be applied at level S if $\sigma < 1/2$ and at level B if $\sigma > 1/2$. We cannot force the surface flux to satisfy the bulk aerodynamic formula and the flux at level B to satisfy (3.5) simultaneously, unless some additional freedom is introduced.

The needed freedom lies in the choice of $\partial\bar{\psi}/\partial z$, which is unknown at this point anyway. We now assume that $\partial\bar{\psi}/\partial z$ is constant with height and drop the time-derivative term of (5.4). This leads to an ordinary differential equation for F_ψ, which, using hydrostatics, can be written as

$$\frac{(1-2\sigma)}{M_c}\left(\frac{\partial F_\psi}{\partial p}-\frac{F_\psi}{\delta p_*}\right)=-\frac{\partial\bar{\psi}}{\partial p}, \tag{5.7}$$

where

$$\delta p_* \equiv \frac{gM_c\hat{\tau}}{\sigma(1-\sigma)(1-2\sigma)}, \tag{5.8}$$

and

$$\hat{\tau} \equiv (1-2\sigma)^2\tau_{\text{dis}}. \tag{5.9}$$

We assume that $\hat{\tau}$ is independent of σ. The motivation for this assumption is explained in appendix C.

The solution of (5.7) is

$$F_\psi = M_c\left[\frac{\delta p_*}{(1-2\sigma)}\frac{\partial\bar{\psi}}{\partial p}+A\exp\left(\frac{p-p_B}{\delta p_*}\right)\right], \tag{5.10}$$

where A is an arbitrary constant. In order to maintain consistency of (5.10) with the imposed fluxes at the top and bottom of the PBL, we must choose appropriate values of $\partial\bar{\psi}/\partial p$ and A. In this way, we find that

$$\frac{\partial\bar{\psi}}{\partial p}=\frac{(1-2\sigma)}{M_c\delta p_*}\left[\frac{(F_\psi)_S-(F_\psi)_B\exp\left(\frac{\delta p_M}{\delta p_*}\right)}{1-\exp\left(\frac{\delta p_M}{\delta p_*}\right)}\right], \tag{5.11}$$

and

$$F_\psi=\left\{(F_\psi)_S\left[1-\exp\left(\frac{p-p_B}{\delta p_*}\right)\right]+(F_\psi)_B\left[\exp\left(\frac{p-p_B}{\delta p_*}\right)-\exp\left(\frac{\delta p_M}{\delta p_*}\right)\right]\right\}\Bigg/\left[1-\exp\left(\frac{\delta p_M}{\delta p_*}\right)\right]. \tag{5.12}$$

The results show how the mean gradient and the flux profile are determined for given values of the fluxes at levels S and B and the other parameters. Note from (5.11) that $\partial\bar{\psi}/\partial p$ vanishes for $\sigma = 1/2$. Inspection of (5.12) confirms that F_ψ satisfies the appropriate boundary conditions at levels S and B.

Obviously, $\delta p_M/\delta p_*$ is a key parameter in (5.11)–(5.12). It can be written as

$$\frac{\delta p_M}{\delta p_*}=\frac{\sigma(1-\sigma)(1-2\sigma)\delta p_M}{gM_c\hat{\tau}}. \tag{5.13}$$

As an example, Fig. 7 shows how $\delta p_M/\delta p_*$ varies with σ, for the particular case $M_c = 0.4$ kg m^{-2} s^{-1}, $\delta p_M = 50$ mb. The solid line is for $\hat{\tau} = 1$ sec, and the dashed line is for $\hat{\tau} = 10$ sec (see appendix C for a discussion of $\hat{\tau}$). Note that $\delta p_M/\delta p_*$ passes through zero for $\sigma = 1/2$. As is apparent from (5.13), $\delta p_M/\delta p_*$ decreases as $\hat{\tau}$ increases. In this example, for $\hat{\tau} = 1$ sec, $\delta p_M/\delta p_*$ can be of order $\pm 10^2$ for σ moderately different from $1/2$. Smaller values of $\delta p_M/\delta p_*$ are favored by a stronger convective mass flux and larger values of $\hat{\tau}$.

Extending this example, Fig. 8 shows how $\partial\bar{\psi}/\partial p$ varies with σ. Again, the solid line is for $\hat{\tau} = 1$ sec, and the dashed line is for $\hat{\tau} = 10$ sec. Here we consider potential temperature θ (Fig. 8a) and the mixing ratio of water vapor q (Fig. 8b). The "edge" fluxes are assumed to be $(F_\theta)_S = 0.1$ kg K m^{-2} s^{-1}, $(F_\theta)_B = -0.02$ kg K m^{-2} s^{-1}, and $(F_q)_S = 3\times10^{-5}$ kg m^{-2} s^{-1} and $(F_q)_B = 2.5\times10^{-5}$ kg m^{-2} s^{-1}. For potential temperature, the results are plotted as K (50 mb)$^{-1}$, and for moisture they are plotted as g kg^{-1} (50 mb)$^{-1}$. The figure shows that the sign of $\partial\bar{\theta}/\partial p$ depends on σ; positive values (upward decrease) occur for $\sigma > 1/2$, and negative values (upward increase) for $\sigma < 1/2$. In contrast, the sign of $\partial\bar{q}/\partial p$ is positive (upward decrease) for all values of σ. The different behaviors of $\partial\bar{\theta}/\partial p$ and $\partial\bar{q}/\partial p$ arise from the differences in their respective prescribed fluxes at levels S and B. With the values of these fluxes that we have prescribed for this example, observations suggest (e.g., Wyngaard and Brost 1984)

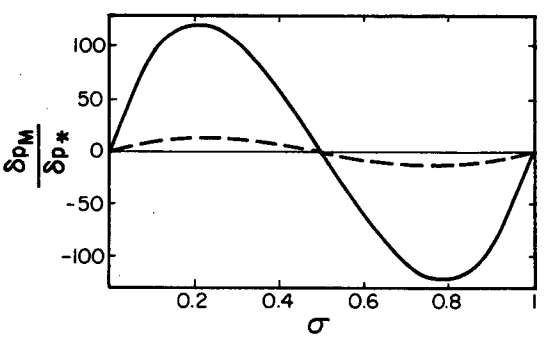

FIG. 7. The variation of $\delta p_M/\delta p_*$ with σ, for the particular case $M_c = 0.4$ kg m^{-2} s^{-1}, $\delta p_M = 50$ mb. The solid line is for $\hat{\tau} = 1$ sec, and the dashed line is for $\hat{\tau} = 10$ sec.

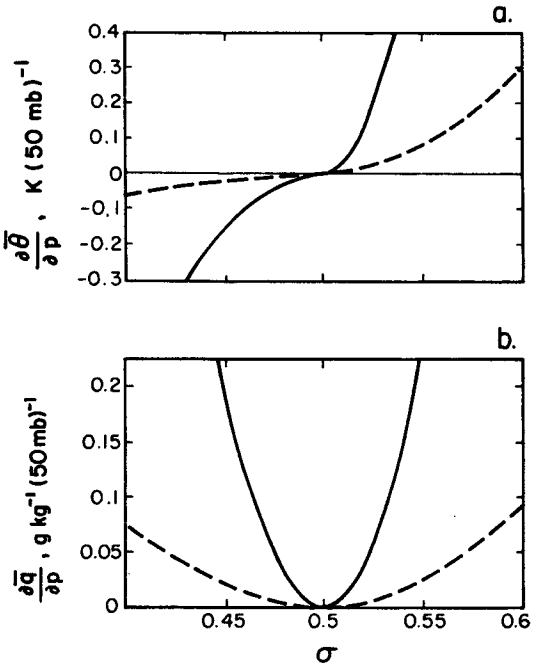

FIG. 8. As in Fig. 7 but for the variation of $\partial\bar{\psi}/\partial p$ with σ: (a) potential temperature in units of K (50 mb)$^{-1}$; (b) the mixing ratio of water vapor in units of g kg^{-1} (50 mb)$^{-1}$.

that potential temperature should increase upward and water vapor mixing ratio should decrease upward. Our model predicts such a result for σ less than 1/2. The numerical values of the vertical gradients are qualitatively reasonable. The gradients become stronger as $\hat{\tau}$ decreases, for a given value of σ.

Figure 9 shows the variations of the fluxes of potential temperature and moisture with height, from the surface to the PBL top. As before, the solid line is for $\hat{\tau} = 1$ sec, and the dashed line is for $\hat{\tau} = 10$ sec. Larger $\hat{\tau}$ favors more linear flux profiles.

As discussed earlier, there is reason to believe that σ is often close to 1/2. For $\delta p_M/\delta p_* \ll 1$, which can be interpreted [see (5.8) or Fig. 7] as σ close to 1/2, (5.12) and (5.11) can be approximated by

$$F_\psi \approx (F_\psi)_B\left(\frac{p_S - p}{\delta p_M}\right) + (F_\psi)_S\left(\frac{p - p_B}{\delta p_M}\right) + \frac{1}{2}\left(\frac{\delta p_M}{\delta p_*}\right)\left(\frac{p - p_B}{\delta p_M}\right)\left(\frac{p_S - p}{\delta p_M}\right) \times [(F_\psi)_B - (F_\psi)_S], \quad (5.14)$$

and

$$\frac{\partial\bar{\psi}}{\partial p} \approx \frac{g\hat{\tau}}{\sigma(1-\sigma)(\delta p_M)^2}\left(\frac{\delta p_M}{\delta p_*}\right) \times \left\{[(F_\psi)_B - (F_\psi)_S] + \frac{1}{2}\frac{\delta p_M}{\delta p_*}[(F_\psi)_B + (F_\psi)_S]\right\}, \quad (5.15)$$

respectively. To obtain (5.15) from (5.11), we have used (5.8). In (5.14) we have kept terms of first order in $\delta p_M/\delta p_*$, while in (5.15) we have kept terms of second order. Since (5.14) is quadratic in p, differentiating it twice with respect to p gives a constant, which is compatible with our assumed constant value of $\partial\bar{\psi}/\partial p$.

According to (5.15), $\partial\bar{\psi}/\partial p$ vanishes for $\sigma = 1/2$, since this is the limit $\delta p_M/\delta p_* \to 0$. In this same limit, (5.14) reduces to the familiar linear flux profile. We conclude that our model reduces to the classical well-mixed layer for $\sigma = 1/2$.

Suppose that F_ψ is independent of height, as in the water vapor example given above. Then (5.15) reduces to

$$\frac{\partial\bar{\psi}}{\partial p} \approx \frac{g\hat{\tau}}{\sigma(1-\sigma)(\delta p_M)^2}\left(\frac{\delta p_M}{\delta p_*}\right)^2 F_\psi. \quad (5.16)$$

For $F_\psi > 0$, as in the case of an upward moisture flux, (5.16) predicts that $\bar{\psi}$ decreases upward. This is consistent with observations showing that the mixing ratio

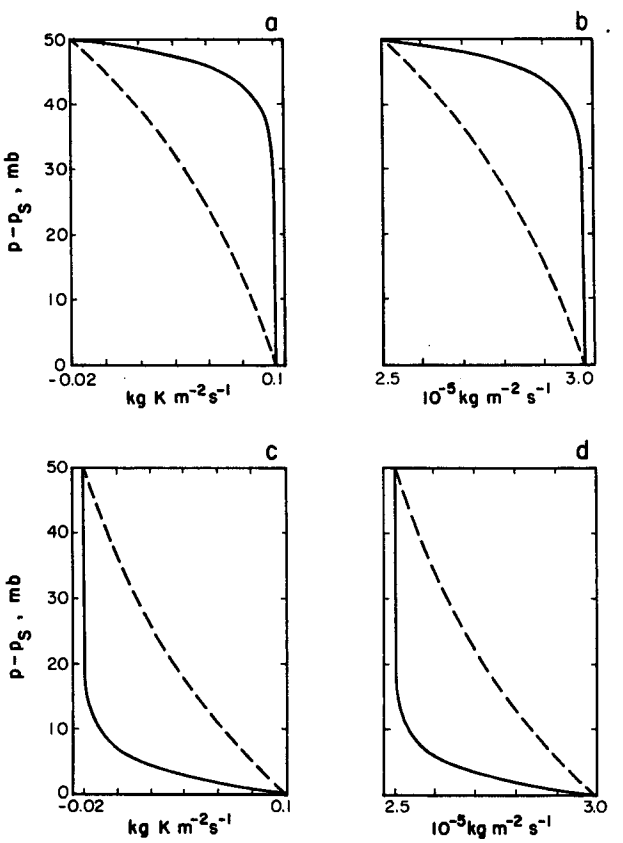

FIG. 9. As in Fig. 7 but for the variations of the fluxes of potential temperature and moisture with height, from the surface to the PBL top: (a) potential temperature flux for $\sigma = 0.52$; (b) moisture flux for $\sigma = 0.52$; (c) potential temperature flux for $\sigma = 0.48$; and (d) moisture flux for $\sigma = 0.48$.

of water vapor typically decreases upward in strongly entraining boundary layers (e.g., Wyngaard and Brost 1984). As a second special case, suppose that $|(F_\psi)_B| \ll |(F_\psi)_S|$, which is typically true for the potential temperature flux in convective PBLs. Then (5.15) reduces to

$$\frac{\partial\bar{\psi}}{\partial p} \approx \frac{-g\hat{\tau}}{\sigma(1-\sigma)(\delta p_M)^2}\left(\frac{\delta p_M}{\delta p_*}\right)\left[1-\frac{1}{2}\left(\frac{\delta p_M}{\delta p_*}\right)\right](F_\psi)_S$$

$$\approx \frac{-g\hat{\tau}}{\sigma(1-\sigma)(\delta p_M)^2}\left(\frac{\delta p_M}{\delta p_*}\right)(F_\psi)_S. \qquad (5.17)$$

For the case of an upward surface potential temperature flux, with $\sigma < \frac{1}{2}$ (i.e., $\delta p_M/\delta p_* > 0$), (5.17) predicts that the potential temperature increases upward, that is, the flux is countergradient; again, this is consistent with observations (e.g., Wyngaard and Brost 1984).

If we truncate (5.15) at first order in $\delta p_M/\delta p_*$, substitute into (5.14), and use (5.9), we obtain

$$F_\psi \approx (F_\psi)_B\left(\frac{p_S-p}{\delta p_M}\right)+(F_\psi)_S\left(\frac{p-p_B}{\delta p_M}\right)$$

$$+\frac{1}{2}\frac{(p-p_B)(p_S-p)\sigma(1-\sigma)}{g\hat{\tau}}\frac{\partial\bar{\psi}}{\partial p}. \qquad (5.18)$$

The first line on the rhs of (5.18) is the linear flux profile characteristic of a well-mixed layer, and the second represents a downgradient diffusion. According to (5.18), when the PBL fluctuates away from a well-mixed structure, the flux profile changes in such a way as to damp the fluctuation. This seems quite plausible.

6. Summary and conclusions

We have presented an internally consistent PBL model that has a parameterized vertical structure but also includes a simple second-order closure.

In section 2, a method is proposed to determine the updraft and downdraft properties applicable to a mass-flux model by using vertical motion statistics obtained from observations, LES, or even higher-order closure. This method cannot be used to determine σ and M_c in a bulk mass-flux model, however, because the needed inputs are not available in such a model.

In section 3, consistency conditions are imposed on the various fluxes, and suitable boundary conditions are applied on the updraft properties at the top of the ventilation layer and the downdraft properties at the base of the entrainment layer to develop simple relationships among mass fluxes, fractional areas, and mixing parameters.

In section 4, methods applicable to the bulk mass-flux model are presented to determine the convective mass flux and σ. So far as we are aware, the results obtained in section 4 represent the first physically based method to determine σ.

By applying the mass-flux model to the interior of the PBL, we obtain, in section 5, an idealized but physically based approach to relaxing the well-mixed assumption that has been such a mainstay of bulk boundary-layer models over the past 25 years or so. In particular, the variance budget equation determines the turbulent fluxes and the gradients of the mean state in the interior of the PBL. These vertical profiles are solved for analytically. Under appropriate conditions, the variance budget equation can reduce to downgradient diffusion or to a "compensating subsidence" formula similar to that used in cumulus parameterizations. This represents a first attempt to marry the approaches of higher-order closure and convective mass-flux closure. Appendix A extends this higher-order closure approach to the entrainment and ventilation layers.

In the future, we hope to generalize the model to allow σ and M_c to vary with height, possibly by following the approach sketched in appendix A.

The variance balance equation presented in section 5 and the TKE prediction equation given in appendix B comprise what amounts to a simple second-order closure, formulated in terms of the mass-flux model and applicable to the bulk boundary-layer model. This approach can be put into perspective as follows.

In recent years, two new approaches have emerged for including the effects of the planetary boundary layer (PBL) in large-scale models. The first involves coupling the large-scale model with a "bulk" PBL model. Advantages of the bulk approach are its simplicity and computational economy. A disadvantage, up to now, is its inability to represent the internal structure of the PBL.

A second approach is to make use of a higher-order closure model in which one or more turbulence variables are prognostically determined. This idea has aroused widespread interest, but has been adopted in practice only by K. Miyakoda's group at the Geophysical Fluid Dynamics Laboratory (Miyakoda and Sirutis 1977; Miyakoda et al. 1983). Advantages of this approach are its relatively high degree of physical sophistication and its ability to predict the internal structure of the PBL. Disadvantages are its requirement for high vertical resolution and its relative complexity. Both of these lead to considerable computational expense.

The present model can be viewed as an attempt to merge these two approaches, retaining the advantages of each and giving rise to what we call a "second-order bulk model" (SOB). Our model also makes use of a convective mass flux, a concept that has been important in the development of cumulus parameterizations. Figure 10 summarizes the conceptual pedigree of our

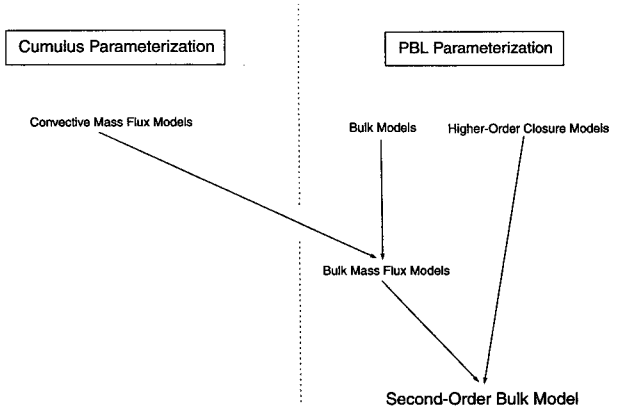

FIG. 10. Diagram summarizing the relationship of the present model to earlier models used in boundary-layer and cumulus parameterizations.

model, relative to earlier models used in boundary-layer and cumulus parameterizations.

Although the approach presented here is highly idealized, it is potentially useful for parameterization and also for physical understanding of the results of more complex models.

Acknowledgments. Dr. V. Lykossov of the Institute of Numerical Mathematics of the Russian Academy of Sciences made very useful suggestions concerning the ideas presented in section 5. The comments of the anonymous reviewers also led to substantial improvements of this paper.

D. Randall has been working on this for longer than he cares to admit. Portions of this research were carried out while he was visiting first the International Meteorological Institute of the University of Stockholm and later the European Centre for Medium-Range Weather Forecasts. Both institutions provided fine working environments. Thanks are due to Drs. Hilding Sundqvist and Gilles Sommeria.

Support for this research was provided by NASA's Climate Program under Grant NAG-1-893 and by the Office of Naval Research under Contract N00014-89-J-1364.

APPENDIX A

Scalar Variance Budgets for the Ventilation and Entrainment Layers

In section 3, we derive constraints on M_c and σ by forcing the convective mass-flux model to be consistent with the fluxes of ψ due to entrainment and ventilation. We now derive additional constraints by use of the conservation principle for ψ'^2, as applied to the ventilation and entrainment layers.

Because $\bar{\psi}$ varies rapidly across the top of the ventilation layer and the base of the entrainment layer, there is vigorous variance production in these regions, but there is also rapid variance dissipation by small eddies. The variance budget for the ventilation layer can be approximated by

$$2\int_{z_{S-}}^{z_S} \epsilon_\psi \rho dz = 2(F_\psi)_S(\bar{\psi}_{S-} - \bar{\psi}_S) - (\rho\overline{w'\psi'\psi'})_S. \tag{A.1}$$

The lhs of (A.1) represents dissipation. The first term on the rhs represents gradient production, and the second represents downward transport into the ventilation layer by triple correlations. We have neglected the terms representing the local time rate of change and advection by the mean flow.

Similarly, the variance budget for the entrainment layer can be expressed as

$$2\int_{z_B}^{z_{B+}} \epsilon_\psi \rho dz = -(F_\psi)_B \Delta\bar{\psi} + (\rho\overline{w'\psi'\psi'})_B - E(\overline{\psi'^2})_B + 2\int_{z_B}^{z_{B+}} \overline{\psi' S'_\psi} dz. \tag{A.2}$$

The lhs and the first two terms on the rhs of (A.2) are closely analogous to those of (A.1). In the gradient production term of (A.2) the minus sign appears because of the definition of $\Delta\bar{\psi}$. The factor of 2 that appears in the production term of (A.1) is not present in the corresponding term of (A.2) because although the turbulent flux of ψ is nearly constant across the ventilation layer, it drops from $(F_\psi)_B$ to zero across the entrainment layer, so that its average value for the entrainment layer is *half* of $(F_\psi)_B$. The second term of (A.2) represents the transport of variance into the entrainment layer by triple correlations. The fourth term represents the rate at which scalar variance is provided to the newly entrained air. The fifth term represents variance production due to fluctuations of S_ψ in the entrainment layer. There is a close analogy between (A.2) and (3.5).

Recall from section 2 that the plume-scale variance of ψ is given by

$$\overline{\psi'^2} = \sigma(1-\sigma)(\psi_u - \psi_d)^2 \tag{A.3}$$

and that the plume-scale variance transport can be written as

$$\rho\overline{w'\psi'\psi'} = M_c(1-2\sigma)(\psi_u - \psi_d)^2. \tag{A.4}$$

For the LES results shown in Fig. 3, σ is so close to 1/2 at both levels S and B that the only safe conclusion is that variance production and dissipation are closely balanced in both the entrainment and ventilation layers. If $(\rho\overline{w'\psi'\psi'})_S = (\rho\overline{w'\psi'\psi'})_B$, the variance flux passes through the interior of the PBL without convergence or divergence.

These ideas may have some relevance to mesoscale cellular convection, if our mass-flux model can be ap-

plied to the mesoscale convective circulations. For the case of open cellular convection, surface heating is believed to dominate (e.g., Arakawa 1975), and observations suggest that $\sigma_B \ll 1$. According to our model, the entrainment layer with $\sigma_B \ll 1$ is dissipating more variance than it produces. This seems physically plausible for open cells. For closed cellular convection, cloud-top cooling is believed to be dominant (Arakawa 1975), and observations suggest that $\sigma_B \approx 1$. According to our model, the entrainment layer with $\sigma_B \approx 1$ is producing more variance than it is dissipating. This seems physically plausible for closed cells.

We now define nondimensional measures of the dissipation rates denoted by k_V and k_E, respectively:

$$2\int_{z_{S-}}^{z_S} \epsilon_\psi \rho dz \equiv k_V V \sigma_S (1-\sigma_S)(\psi_u - \psi_d)_S^2, \quad \text{(A.5)}$$

$$2\int_{z_B}^{z_{B+}} \epsilon_\psi \rho dz \equiv k_E E \sigma_B (1-\sigma_B)(\psi_u - \psi_d)_B^2. \quad \text{(A.6)}$$

Rapid variance dissipation rates in the ventilation and entrainment layers correspond to large values of k_V and k_E, respectively. Note from (A.3) that the rhs of (A.5) and (A.6) are proportional to $\overline{\psi'^2}$ for the ventilation and entrainment layers, respectively. The definitions of k_V and k_E, given by (A.5) and (A.6), are motivated by the idea that the rates of variance dissipation in the ventilation and entrainment layers should be related to the actual values of the variances at the edges of those layers.

Using the results of section 3 with (A.4) and (A.5), we rewrite (A.1) as

$$\sigma_S = \frac{2 - \chi_V}{k_V \chi_V^2 + 2(1-\chi_V)}. \quad \text{(A.7)}$$

All reference to ψ has dropped out of (A.7), indicating that k_V is independent of species.

Now turning to the entrainment layer, we can use (A.3), (A.4), and (A.6) with the results of section 3 to rewrite (A.2) as

$$\begin{aligned}(\psi_u - \psi_d)_B^2 \chi_E M_{c,B} \{ &-k_E(1-\sigma_B) \\ &+ \chi_E^{-1}[\chi_E^{-1}\sigma_B + (1-2\sigma_B)] - (1-\sigma_B)\} \\ &+ (\psi_u - \psi_d)_B \frac{M_{c,B}}{E}\int_{z_B}^{z_{B+}} \overline{S_\psi} dz \\ &+ 2\int_{z_B}^{z_{B+}} \overline{\psi' S'_\psi} dz = 0. \quad \text{(A.8)}\end{aligned}$$

We require that (A.8) hold for all species, including those for which S_ψ is zero. It follows that

$$\sigma_B = \frac{k_E \chi_E^2 - \chi_E + \chi_E^2}{1 + k_E \chi_E^2 - 2\chi_E + \chi_E^2}. \quad \text{(A.9)}$$

Again, all reference to ψ has dropped out, showing that k_E is independent of species.

Since (A.8) and (A.9) must apply for all species, including those for which S_ψ is not zero, we conclude that

$$2\int_{z_B}^{z_{B+}} \overline{\psi' S'_\psi} dz = -\frac{(F_\psi)_B}{E_B}\int_{z_B}^{z_{B+}} \overline{S_\psi} dz. \quad \text{(A.10)}$$

Using (A.10), we can determine the rate at which fluctuations of S_ψ in the entrainment layer generate fluctuations of ψ there.

Using the results derived above, we can show that the ratio of dissipation to production, for the ventilation layer satisfies

$$\frac{2\int_{z_{S-}}^{z_S} \epsilon_\psi \rho dz}{2(F_\psi)_S(\bar{\psi}_{S-} - \bar{\psi}_S)} = 1 - \left[\frac{\chi_V(1-2\sigma_S)}{2(1-\sigma_S)}\right]. \quad \text{(A.11)}$$

The corresponding ratio for the entrainment layer is

$$\begin{aligned}&\frac{2\int_{z_B}^{z_{B+}} \epsilon_\psi \rho dz}{-(F_\psi)_B \Delta\psi - E(\overline{\psi'^2})_B + 2\int_{z_B}^{z_{B+}} \overline{\psi' S'_\psi} dz} \\ &\qquad = 1 + \left[\frac{\chi_E(1-2\sigma_B)}{\sigma_B - \chi_E^2(1-\sigma_B)}\right]. \quad \text{(A.12)}\end{aligned}$$

Note from (A.11) and (A.12) that, since χ_V and χ_E are both on the order of 10^{-2}, and if σ is close to $1/2$, dissipation and production must nearly balance in the ventilation and entrainment layers. Such near balances are observed (e.g., Caughey and Palmer 1979) and have been predicted through LES (see for example Fig. 7 of Moeng and Wyngaard 1989).

Now combine (A.7) with (3.4) to obtain a quadratic equation for χ_V. The solutions, which are both physically relevant, are given by

$$\chi_V = \frac{2G_\nu + k_V \pm \sqrt{k_V^2 - 8G_V^2 k_V + 4G_V^2}}{2k_V G_V}. \quad \text{(A.13)}$$

Using (3.4), we can obtain the corresponding solutions for σ_S:

$$\sigma_S = \frac{(k_V - 2G_\nu) \mp \sqrt{k_V^2 - 8G_V^2 k_V + 4G_V^2}}{2k_V}. \quad \text{(A.14)}$$

The condition that the discriminant in (A.13) and (A.14) be nonnegative implies that k_V must be sufficiently large for a given G_V. The discriminant vanishes for

$$k_V = (k_V)_{\min} = 4G_V^2 + 2G_V\sqrt{4G_V^2 - 1}. \quad \text{(A.15)}$$

For convenience, let

$$r_V \equiv \frac{k_V}{(k_V)_{\min}}. \tag{A.16}$$

Figure 11 shows plots of χ_V and σ_S against G_V and r_V. Both solutions are shown. Note that for sufficiently large G_V, σ_S depends only on r_V. For $G_V \gg 1$, the following approximate relations hold:

$$(k_V)_{\min} \approx 8G_V^2, \tag{A.17}$$

$$\sigma_S \approx \frac{r_V \mp \sqrt{r_V(r_V-1)}}{2r_V}, \tag{A.18}$$

$$\chi_V \approx \frac{r_V \pm \sqrt{r_V(r_V-1)}}{2r_V G_V}. \tag{A.19}$$

From (A.18) we conclude that

$$\tfrac{1}{2} \leq \sigma_S \leq 1 \quad \text{with the choice of the minus, or}$$

$$0 \leq \sigma_S \leq \tfrac{1}{2} \quad \text{with the choice of the plus.} \tag{A.20}$$

By substituting (A.17)–(A.19) back into (A.1) and (A.5), we can show that the approximation $G_V \gg 1$, on which (A.17)–(A.19) are based, corresponds to a balance between dissipation and production.

A parallel analysis for the entrainment layer leads to

$$\chi_E = \frac{2G_E + k_E + 1 \pm k_E^2\sqrt{k_E^2 + (2-4G_E^2)k_E + 1}}{2G_E(1+k_E)} \tag{A.21}$$

and

$$\sigma_B = \frac{2G_E + k_E + 1 \pm k_E^2\sqrt{k_E^2 + (2-4G_E^2)k_E + 1}}{2(1+k_E)}. \tag{A.22}$$

Again, both solutions are physically relevant. The condition that the discriminant in (A.21) and (A.22) be nonnegative implies that k_E must be sufficiently large. The discriminant vanishes for

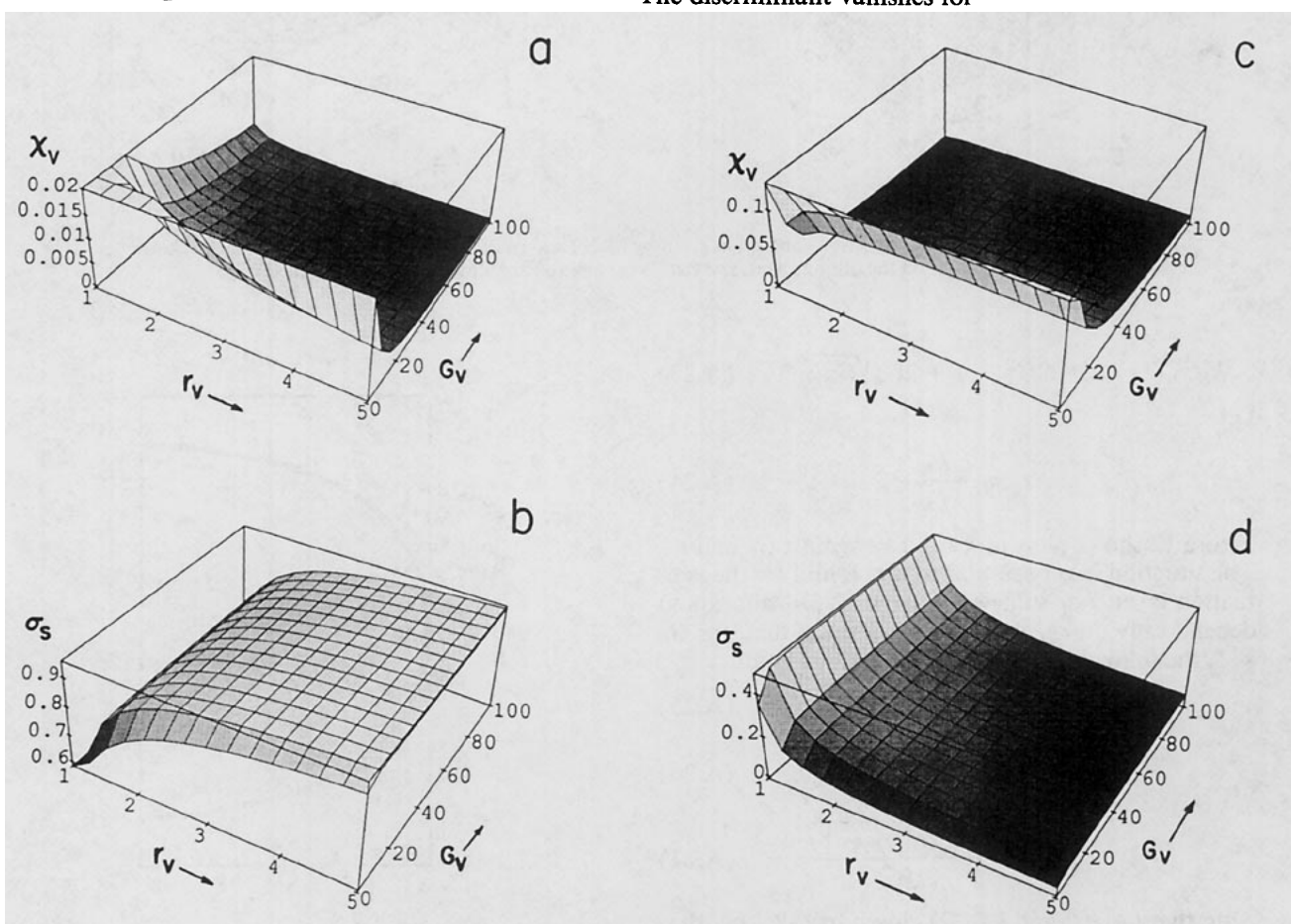

FIG. 11. Plots of χ_V and σ_S against k_V and r_V, as given by (4.13) and (4.15). Panels (a) and (b) are for the choice of the plus sign on the discriminant, and panels (c) and (d) are for the choice of the minus sign.

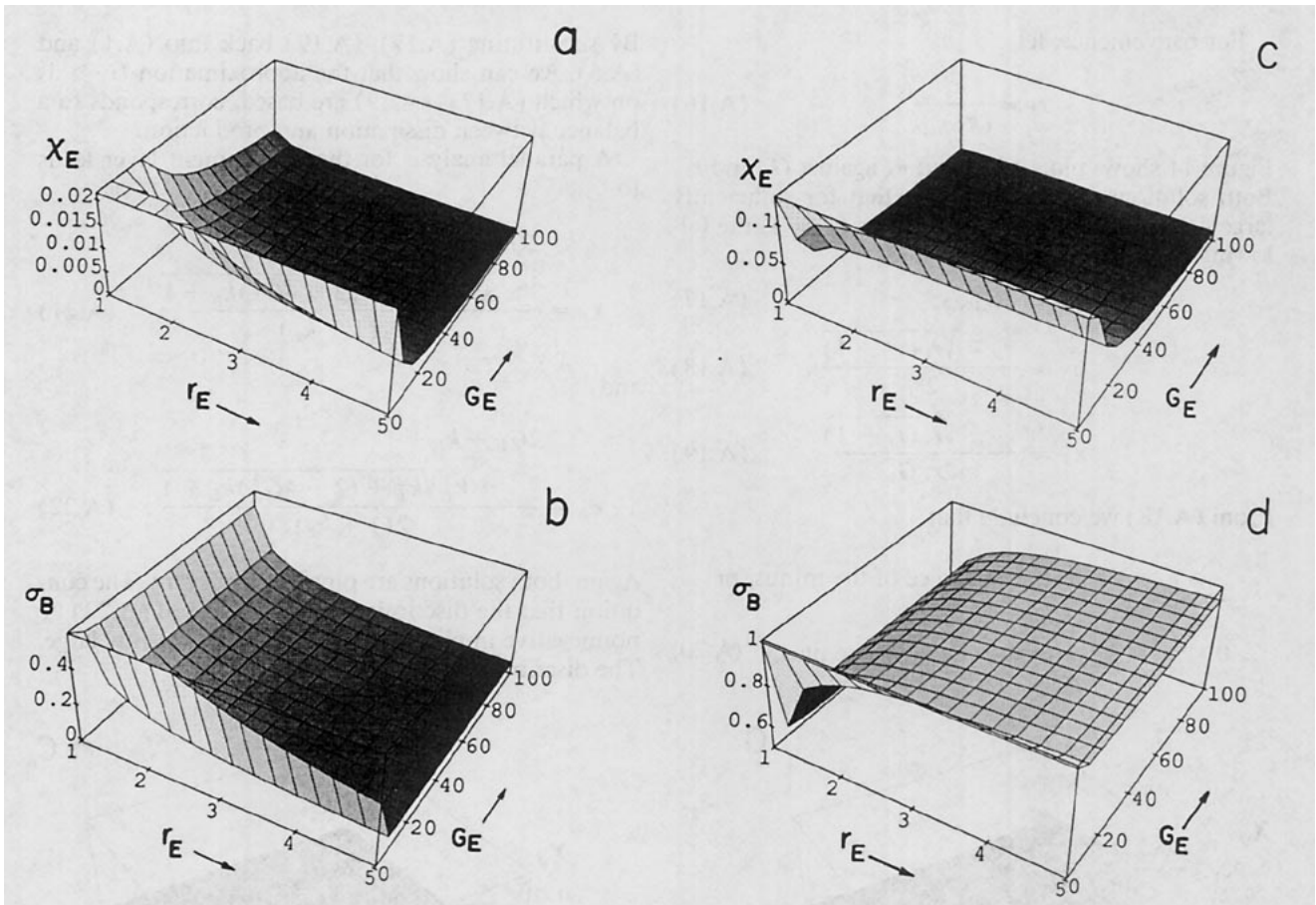

FIG. 12. Plots of χ_E and σ_B against k_E and r_E, as given by (4.21) and (4.22). Panels (a) and (b) are for the choice of the plus sign on the discriminant, and panels (c) and (d) are for the choice of the minus sign.

$$k_E = (k_E)_{\min} = 2G_E^2 - 1 + 2G_E\sqrt{G_E^2 - 1}. \quad \text{(A.23)}$$

Let

$$r_E \equiv \frac{k_E}{(k_E)_{\min}}. \quad \text{(A.24)}$$

Figure 12 shows plots of χ_E and σ_B against G_E and r_E. The situation is very similar to that found for the ventilation layer. For sufficiently large G_E, σ_B appears to depend only on r_E. We can demonstrate that, for $G_E \gg 1$, the following approximate relations hold:

$$(k_E)_{\min} \approx 4G_E^2 \quad \text{(A.25)}$$

$$\sigma_B \approx \frac{r_E \pm \sqrt{r_E(r_E - 1)}}{2r_E}, \quad \text{(A.26)}$$

$$\chi_E \approx \frac{r_E \pm \sqrt{r_E(r_E - 1)}}{2r_E G_E}. \quad \text{(A.27)}$$

Note that (A.26) and (A.27) closely parallel (A.19). Figure 13 shows σ_B as a function of r_E, and/or σ_S as a function of r_V, as given by (A.18) and/or (A.26).

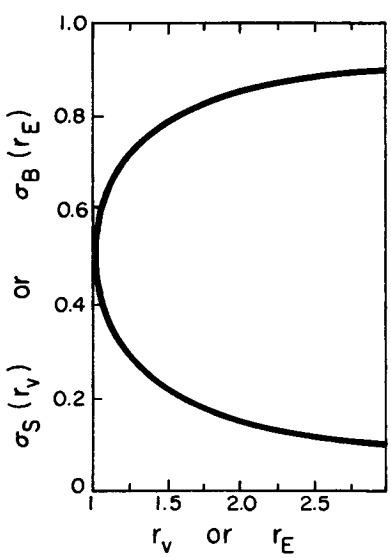

FIG. 13. Plot of σ_B as a function of r_E, or of σ_S, or of both, as a function of r_V.

From (A.26), we can conclude that

$$\frac{1}{2} \leq \sigma_B \leq 1 \quad \text{with the choice of the plus, and}$$

$$0 \leq \sigma_B \leq \frac{1}{2} \quad \text{with the choice of the minus.} \tag{A.28}$$

The main results of this appendix are (A.18) and (A.19) and (A.26) and (A.29). Our expressions for σ_S and σ_B automatically satisfy $0 < \sigma < 1$. If r_V and r_E were known, we could find σ_S, σ_B, and χ_E and χ_E. The values of $M_{c,S}$ and $M_{c,B}$ would follow immediately from (3.4) and (3.9), respectively. The interior value of M_c could be obtained by an approach analogous to that used in section 4. We would thus be in a position to allow σ to vary linearly with height and M_c to vary quadratically. This would allow improved agreement with the LES results presented in Fig. 3. Pursuit of this generalization of our model is left to the future.

APPENDIX B

A Method to Predict the Vertically Integrated Turbulence Kinetic Energy

The vertically integrated conservation law for the TKE can be written as

$$g^{-1}\delta p_M \frac{\partial e_M}{\partial t} + E e_M = B + S - D. \tag{B.1}$$

Here B, S, and D represent production by buoyancy, production by shear, and dissipation, respectively, and δp_M is the pressure thickness of the PBL.

The vertically integrated dissipation rate and the vertically averaged TKE are assumed to be related by

$$D = \rho_M (e_M / a_1)^{3/2}, \tag{B.2}$$

where ρ_M is the vertically averaged PBL density and $a_1 \approx 0.163$ is a dimensionless constant.

The buoyancy production integral B is of the form

$$B = \kappa \int_{p_{B+}}^{p_{S-}} \frac{F_{Sv}}{p}\, dp, \tag{B.3}$$

where κ is Poisson's constant. This integral can be evaluated using the methods of Randall (1984).

The shear production integral S is of the form

$$S = \int_{p_{B+}}^{p_{S-}} \mathbf{F}_V \cdot \frac{\partial \bar{\mathbf{V}}}{\partial p}\, dp. \tag{B.4}$$

We divide this integral into three parts: shear production in the surface layer, shear production in the interior of the PBL, and shear production in the entrainment layer. The surface-layer shear production is approximately given by

$$\int_{p_S}^{p_{S-}} \mathbf{F}_V \cdot \frac{\partial \bar{\mathbf{V}}}{\partial p}\, dp = (\mathbf{F}_V)_S \cdot \bar{\mathbf{V}}_S = |(\mathbf{F}_V)_S| \cdot |\bar{\mathbf{V}}_S|. \tag{B.5}$$

Here the second equality follows from the assumption that the surface stress is parallel to the surface wind.

The interior shear production can be evaluated by straightforward methods once the profiles of the stress and the wind are known.

Finally, the entrainment-layer shear production is approximately given by

$$\int_{p_{B+}}^{p_B} \mathbf{F}_V \cdot \frac{\partial \bar{\mathbf{V}}}{\partial p}\, dp = \frac{1}{2} |(\mathbf{F}_V)_B| \cdot |\Delta \bar{\mathbf{V}}| = \frac{1}{2} E |\Delta \bar{\mathbf{V}}|^2. \tag{B.6}$$

In (B.6), the factor of 1/2 arises because $\mathbf{F}_V$ decreases from $(\mathbf{F}_V)_B$ to zero across the entrainment layer, so that its average value inside the entrainment layer is $(\mathbf{F}_V)_B/2$. The second equality comes from applying (3.5) to the momentum budget of the entrainment layer.

APPENDIX C

Motivation for (5.8)–(5.9)

Dropping the time dependence of (5.3) and simplifying, we obtain

$$\frac{(1-2\sigma)}{M_c} \frac{\partial F_\psi}{\partial p} - \frac{\sigma(1-\sigma)}{g\tau_{\text{dis}} M_c^2} F_\psi = -\frac{\partial \bar{\psi}}{\partial p}. \tag{C.1}$$

This is basically the same as (5.7) except that we have not introduced δp_*. We solve (C.1) as a first-order ordinary differential equation for F_ψ, assuming constant coefficients and a constant value of $\partial\bar{\psi}/\partial p$. The solution is

$$F_\psi = \frac{g\tau_{\text{dis}} M_c^2}{\sigma(1-\sigma)} \frac{\partial \bar{\psi}}{\partial p} + A \exp\left[\frac{\sigma(1-\sigma)(p-p_B)}{g\tau_{\text{dis}} M_c (1-2\sigma)}\right], \tag{C.2}$$

where A is the constant of integration. Notice that the quantity $(1-2\sigma)$ appears in the denominator of the argument of the exponential. As σ passes through 1/2, the argument of the exponential diverges to plus and minus infinity—unacceptable behavior. We cannot solve this problem by choosing $A = 0$ because then F_ψ would be independent of height and could not satisfy its boundary conditions at the surface and the PBL top.

Our interpretation is that τ_{dis} must depend on σ. This is acceptable, since the σ dependence of τ_{dis} is not known a priori. *We choose the σ dependence of τ_{dis} in such a way that F_ψ varies continuously with σ.*

This we can do by taking τ_{dis} proportional to $(1-2\sigma)$; that is,

$$\hat{\tau} \equiv (1 - 2\sigma)\tau_{\text{dis}}, \tag{C.3a}$$

where $\hat{\tau}$ is a constant (i.e., independent of σ). Then (C.2) is replaced by

$$F_\psi = \frac{M_c \delta p_*}{(1 - 2\sigma)} \frac{\partial \bar{\psi}}{\partial p} + A \exp\left[\frac{(p - p_B)}{\delta p_*}\right], \tag{C.4a}$$

where

$$\delta p_* = \frac{g\hat{\tau} M_c}{\sigma(1 - \sigma)}. \tag{C.5a}$$

Inspection of (C.4a) shows that the flux does indeed vary continuously with σ. This approach is unacceptable, however, because (C.3a) will inevitably give negative and hence physically impossible values of τ_{dis} for some values of σ.

We can ensure nonnegative τ_{dis} and also make F_ψ vary continuously with σ by choosing

$$\hat{\tau} \equiv (1 - 2\sigma)^2 \tau_{\text{dis}}, \tag{C.3b}$$

with $\hat{\tau}$ positive and independent of σ. The solution of (C.1) is then

$$F_\psi = M_c\left[\frac{\delta p_*}{(1 - 2\sigma)} \frac{\partial \bar{\psi}}{\partial p} + A \exp\left(\frac{p - p_B}{\delta p_*}\right)\right], \tag{C.4b}$$

where

$$\delta p_* \equiv \frac{g M_c \hat{\tau}}{\sigma(1 - \sigma)(1 - 2\sigma)}. \tag{C.5b}$$

We have used (C.3b) and (C.5b) in section (5).

This is the line of reasoning that led us to adopt (5.9), with $\hat{\tau}$ independent of σ.

An implication of (5.9) is that τ_{dis} becomes infinite (that is, the variance dissipation rate goes to zero) for $\sigma = 1/2$. Of course, this is at best an idealization of how nature works. From the LES results, we estimate that $(1 - 2\sigma) \sim 10^{-1}$ or 10^{-2}, which, together with the results shown in Fig. 6, suggests that for this particular case $\hat{\tau}$ is on the order of 1–10 sec.

Why should τ_{dis} increase as σ approaches 1/2? A possible physical interpretation is that the largest (absolute) convective vertical velocities increase as σ departs from 1/2. For example, if $\sigma \ll 1$, the *updraft* vertical velocities must be relatively vigorous, implying strong lateral shears and suggesting strong lateral mixing and variance dissipation. Similarly, for σ close to unity, the *downdraft* vertical velocities must be relatively vigorous. The intensity of the individual drafts is minimized for $\sigma = 1/2$, suggesting that the dissipation rate is minimized then too.

We must also ask why $\hat{\tau}$ is so short. From (5.2) and (5.9) the dissipation rate can be written as

$$\epsilon_\psi = (1 - 2\sigma)^2\left(\frac{\overline{\psi'^2}}{\hat{\tau}}\right). \tag{C.6}$$

We can interpret $\overline{\psi'^2}/\hat{\tau}$ as the intense *local* dissipation rate in those portions of the convective circulations where dissipation actually occurs and $(1 - 2\sigma)^2$ as the fraction of the domain within which dissipation is localized. The volume-averaged dissipation rate is then given by (C.6).

REFERENCES

Albrecht, B. A., 1979: A model of the thermodynamic structure of the trade-wind boundary layer: Part II. Applications. *J. Atmos. Sci.*, **36**, 90–98.

——, R. S. Penc, and W. H. Schubert, 1985: An observational study of cloud-topped mixed layers. *J. Atmos. Sci.*, **42**, 800–822.

Arakawa, A., 1969: Parameterization of cumulus convection. *Proc. WMO/IUGG Symp. Numerical Weather Prediction,* Tokyo, Japan Meteor. Agency. IV, 8, 1–6.

——, 1975: Modeling clouds and cloud processes for use in climate models. *The Physical Basis of Climate and Climate Modelling.* GARP Publ. Ser. No. 16, ICSU/WMO, Geneva, 181–197.

Benoit, R., 1976: A comprehensive parameterization of the atmospheric boundary layer for general circulation models. Ph.D. dissertation, McGill University, and National Center for Atmospheric Research cooperative thesis No. 39, 278 pp.

Betts, A. K., 1973: Non-precipitating cumulus convection and its parameterization. *Quart. J. Roy. Meteor. Soc.*, **99**, 178–196.

——, 1983: Thermodynamics of mixed stratocumulus layers: Saturation point budgets. *J. Atmos. Sci.*, **40**, 2655–2670.

Caughey, S. J., and S. G. Palmer, 1979: Some aspects of turbulence structure through the depth of the convective boundary layer. *Quart. J. Roy. Meteor. Soc.*, **105**, 811–827.

——, B. A. Crease, and W. T. Roach, 1982: A field study of nocturnal stratocumulus: II. Turbulence structure and entrainment. *Quart. J. Roy. Meteor. Soc.*, **108**, 125–144.

Chatfield, R. B., and R. A. Brost, 1987: A two-stream model of the vertical transport of trace species in the convective boundary layer. *J. Geophys. Res.*, **92**, 13 263–13 276.

Coulman, C. E., 1978: Boundary-layer evolution and nocturnal inversion dispersal, Part II. *Bound-Layer Meteor.*, **14**, 493–513.

Deardorff, J. W., 1972: Parameterization of the planetary boundary layer for use in general circulation models. *Mon. Wea. Rev.*, **100**, 93–106.

Greenhut, G. K., and S. J. S. Khalsa, 1982: Updraft and downdraft events in the atmospheric boundary layer over the equatorial Pacific Ocean. *J. Atmos. Sci.*, **39**, 1803–1818.

Grossman, R. L., 1984: Bivariate conditional sampling of moisture flux over a tropical ocean. *J. Atmos. Sci.*, **41**, 3238–3253.

Hanson, H. P., 1981: On mixing by trade-wind cumuli. *J. Atmos. Sci.*, **38**, 1003–1014.

Khalsa, S. J. S., and G. K. Greenhut, 1985: Conditional sampling of updrafts and downdrafts in the marine atmospheric boundary layer. *J. Atmos. Sci.*, **42**, 2550–2562.

Lamb, R. G., 1978: A numerical simulation of dispersion from an elevated point source in the convective planetary boundary layer. *Atmos. Environ.*, **12**, 1297–1304.

Lenschow, D. H., and P. L. Stephens, 1980: The role of thermals in the convective boundary layer. *Bound.-Layer Meteor.*, **19**, 509–532.

——, and ——, 1982: Mean vertical velocity and turbulence intensity inside and outside thermals. *Atmos. Environ.*, **16**, 761–674.

Lilly, D. K., 1968: Models of cloud-topped mixed layers under a strong inversion. *Quart. J. Roy. Meteor. Soc.*, **94**, 292–309.

Mahrt, L., and J. Paumier, 1984: Heat transport in the atmospheric boundary layer. *J. Atmos. Sci.*, **41**, 3061–3075.

Manton, M. J., 1977: On the structure of convection. *Bound.-Layer Meteor.*, **12**, 491–503.

Moeng, C.-H., 1984: A large-eddy simulation model for the study of

planetary boundary-layer turbulence. *J. Atmos. Sci.*, **41,** 2052–2062.

——, 1986: Large-eddy simulation of a stratus-topped boundary layer. Part 1: Structure and budgets. *J. Atmos. Sci.*, **43,** 2886–2900.

——, and J. C. Wyngaard, 1989: Evaluation of turbulent transport and dissipation closures in second-order modeling. *J. Atmos. Sci.*, **46,** 2311–2330.

——, and R. Rotunno, 1990: Vertical-velocity skewness in the buoyancy-driven boundary layer. *J. Atmos. Sci.*, **47,** 1149–1162.

——, and U. Schumann, 1991: Composite structure of plumes in stratus-topped boundary layers. *J. Atmos. Sci.*, **48,** 2280–2291.

Nicholls, S., 1989: The structure of radiatively driven convection in stratocumulus. *Quart. J. Roy. Meteor. Soc.*, **115,** 487–511.

——, and J. D. Turton, 1986: An observational study of the structure of stratiform cloud sheets. Part II. Entrainment. *Quart. J. Roy. Meteor. Soc.*, **112,** 461–480.

Penc, R. S., and B. A. Albrecht, 1986: Parametric representation of heat and moisture fluxes in cloud-topped mixed layers. *Bound.-Layer Meteor.*, **38,** 225–248.

Randall, D. A., 1976: The interaction of the planetary boundary layer with large-scale circulations. Ph.D. thesis, University of California, Los Angeles, 247 pp.

——, 1987: Turbulent fluxes of liquid water and buoyancy in partly cloudy layers. *J. Atmos. Sci.*, **44,** 850–858.

——, J. A. Abeles, and T. G. Corsetti, 1985: Seasonal simulations of the planetary boundary layer and boundary-layer stratocumulus clouds with a general circulation model. *J. Atmos. Sci.*, **42,** 641–676.

Rayment, R., and C. J. Readings, 1974: A case study of the structure and energetics of an inversion. *Quart. J. Roy. Meteor. Soc.*, **100,** 221–233.

Schmidt, H., and U. Schumann, 1989: Coherent structure of the convective boundary layer derived from large-eddy simulations. *J. Fluid Mech.*, **200,** 511–562.

Schumann, U., and C.-H. Moeng, 1991a: Plume fluxes in clear and cloudy convective boundary layers. *J. Atmos. Sci.*, **48,** 1746–1757.

——, and ——, 1991b: Plume budgets in clear and cloudy convective boundary layers. *J. Atmos. Sci.*, **48,** 1758–1770.

Siems, S. T., C. S. Bretherton, M. B. Baker, S. Shy, and R. T. Breidenthal, 1990: Buoyancy reversal and cloudtop entrainment instability. *Quart. J. Roy. Meteor. Soc.*, **116,** 705–739.

Suarez, M. J., A. Arakawa, and D. A. Randall, 1983: Parameterization of the planetary boundary layer in the UCLA general circulation model: Formulation and results. *Mon. Wea. Rev.*, **111,** 2224–2243.

Wang, S., and B. A. Albrecht, 1986: A stratocumulus model with an internal circulation. *J. Atmos. Sci.*, **43,** 2374–2391.

——, and ——, 1990: A mean-gradient model of the dry convective boundary layer. *J. Atmos. Sci.*, **46,** 126–138.

Wilczak, J. M., and J. A. Businger, 1983: Thermally indirect motions in the convective atmospheric boundary layer. *J. Atmos. Sci.*, **40,** 343–358.

Wyngaard, J. C., and R. A. Brost, 1984: Top-down and bottom-up diffusion of a scalar in the convective boundary layer. *J. Atmos. Sci.*, **41,** 102–112.

Young, G. S., 1988a: Turbulence structure of the convective boundary layer. Part II: Phoenix 78 aircraft observations of thermals and their environment. *J. Atmos. Sci.*, **45,** 727–735.

——, 1988b: Turbulence structure of the convective boundary layer. Part III: The vertical velocity budgets of thermals and their environment. *J. Atmos. Sci.*, **45,** 2039–2049.